RESOURCE

nature neuroscience

A toolbox of Cre-dependent optogenetic transgenic mice for light-induced activation and silencing

Linda Madisen[1], Tianyi Mao[2,7], Henner Koch[3], Jia-min Zhuo[4], Antal Berenyi[5], Shigeyoshi Fujisawa[5], Yun-Wei A Hsu[3], Alfredo J Garcia III[3], Xuan Gu[4], Sebastien Zanella[3], Jolene Kidney[1], Hong Gu[1], Yimei Mao[4], Bryan M Hooks[2], Edward S Boyden[6], György Buzsáki[5], Jan Marino Ramirez[3], Allan R Jones[1], Karel Svoboda[2], Xue Han[4], Eric E Turner[3] & Hongkui Zeng[1]

Cell type–specific expression of optogenetic molecules allows temporally precise manipulation of targeted neuronal activity. Here we present a toolbox of four knock-in mouse lines engineered for strong, Cre-dependent expression of channelrhodopsins ChR2-tdTomato and ChR2-EYFP, halorhodopsin eNpHR3.0 and archaerhodopsin Arch-ER2. All four transgenes mediated Cre-dependent, robust activation or silencing of cortical pyramidal neurons *in vitro* and *in vivo* upon light stimulation, with ChR2-EYFP and Arch-ER2 demonstrating light sensitivity approaching that of *in utero* or virally transduced neurons. We further show specific photoactivation of parvalbumin-positive interneurons in behaving ChR2-EYFP reporter mice. The robust, consistent and inducible nature of our ChR2 mice represents a significant advance over previous lines, and the Arch-ER2 and eNpHR3.0 mice are to our knowledge the first demonstration of successful conditional transgenic optogenetic silencing. When combined with the hundreds of available Cre driver lines, this optimized toolbox of reporter mice will enable widespread investigations of neural circuit function with unprecedented reliability and accuracy.

A major challenge in neuroscience is to understand how brain functions are mediated by particular cell types within neural networks. Dissection of such complex networks requires the ability to manipulate the activities of specific cell types and to examine the resulting effects. A recent innovation in experimental neuroscience has been the development of light-activated channels or pumps, derived from microbial photosynthetic systems, to modulate neural activity, known as optogenetics. The best-known prototypes for the application of optical control in neurons include the neuron-activating cation channel channelrhodopsin-2 (ChR2)[1–3], and the neuron-silencing chloride transporter halorhodopsin (NpHR)[4,5] and proton pump archaerhodopsin-3 (Arch)[6]. These and related optogenetic molecules[7] allow activation or silencing of neurons with unprecedented specificity and excellent temporal precision on a millisecond scale, and are in widespread use.

In mice, cell type–specific genetic manipulation is most widely achieved through the Cre/*lox*P recombinase system. Hundreds of Cre mouse lines, generated in individual labs and through large-scale efforts[8–10], have been established to direct specific gene expression or deletion in a wide range of cell types or populations throughout the nervous system. A challenge in developing optogenetic tools is the need to express high levels of the opsins, owing to the relatively small optical current mediated by each opsin molecule. For this reason, opsin genes have been most often introduced *in vivo* using recombinant viral vectors or by *in utero* electroporation (IUE). By delivering an adeno-associated virus (AAV) that expresses an opsin in a Cre-dependent manner—for example, using *lox*P-flanked ('floxed')-stop or floxed-inverse (FLEX) cassettes[11,12]—it is possible to virally deliver an opsin to a brain region, where only Cre-positive cells will activate expression of the opsin. Although successful for many applications, these approaches possess intrinsic limitations. They can result in incomplete coverage of neurons within the region, which may limit experiments requiring complete labeling (for example, neural silencing), and can result in variable opsin expression levels across cells from the injection center out. The variability in the number and location of opsin-expressing cells between animals necessitates laborious validation for each animal, introducing variability in data interpretation. The brain targets of interest may be very small, very large or hard for the virus to access for other reasons (for example, a difficult location for injection or a particular cell type that cannot be infected by any serotype of virus or cannot be infected during brain development).

A transgenic mouse approach can overcome many of these limitations. However, exogenous opsin gene expression in transgenics is typically regulated by a specific linked promoter and thus is predetermined to occur in a particular and fixed cell population[13–19]. A Cre-dependent system of opsin expression would exploit the abundant resource that available Cre-driver lines constitute and would offer a powerful approach for controlling the activity of a wide range of cells. However, transgenic mice with robust Cre-dependent expression of

[1]Allen Institute for Brain Science, Seattle, Washington, USA. [2]Howard Hughes Medical Institute, Janelia Farm Research Campus, Ashburn, Virginia, USA. [3]Center for Integrative Brain Research, Seattle Children's Research Institute, Seattle, Washington, USA. [4]Department of Biomedical Engineering, Boston University, Boston, Massachusetts, USA. [5]Center for Molecular and Behavioral Neuroscience, Rutgers University, Newark, New Jersey, USA. [6]Media Lab, Massachusetts Institute of Technology, Cambridge, Massachusetts, USA. [7]Present address: Vollum Institute, Oregon Health and Science University, Portland, Oregon, USA. Correspondence should be addressed to H.Z. (hongkuiz@alleninstitute.org).

Received 20 December 2011; accepted 28 February 2012; published online 25 March 2012; doi:10.1038/nn.3078

opsins have been difficult to generate, as indicated by recent characterization of a ChR2 Cre reporter[20]. To our knowledge, no transgenic line with Cre-dependent expression of a silencing opsin has yet been described. However, efforts to overcome the limitations of early versions of silencing opsins, such as protein aggregation and low conductance[21], have led to the development of newer optical silencing molecules, including eNpHR (ref. 22), eNpHR3.0 (ref. 23) and various forms of Arch[6,24], with great improvement in membrane expression and related increase in photoconductance, making reliable genetic silencing achievable now.

Here we report the creation of a toolbox of four new mouse lines with high-level and Cre-dependent expression of the fluorescently tagged ChR2(H134R)-tdTomato, ChR2(H134R)-EYFP, Arch-EGFP-ER2, or eNpHR3.0-EYFP. Inducible expression of these opsins is driven by a specially designed expression cassette in a modified *Rosa26* locus, which we recently showed capable of mediating efficient fluorescent labeling[9]. Here we demonstrate that high-performance optogenetic manipulation in Cre-dependent transgenic mice is enabled for all the classes of opsin molecules using this optimized strategy.

For all four lines, we found that cortical pyramidal neurons were highly responsive to either light activation (ChR2s) or light inhibition (eNpHR3.0, Arch-ER2), in both *in vitro* brain slice preparations and *in vivo* brains of awake animals. In addition, we readily achieved light activation of hippocampal and reticular parvalbumin (*Pvalb*)-positive interneurons, as well as cortical rhythms resulting from synchronized reticular *Pvalb*$^+$ neuron activation, in behaving ChR2-EYFP mice. These results demonstrate that selective optical activation and silencing can be applied to different cell types in different brain regions in these mice, using a variety of photostimulation protocols. Thus, when combined with the many publicly available Cre driver lines, these transgenics should greatly facilitate the study of various neuronal cell types, including those inaccessible to previous approaches.

RESULTS

Generation of mice conditionally expressing opsin genes

We previously demonstrated strong, ubiquitous, Cre-dependent expression of fluorescent markers from a modified *Rosa26* locus by incorporating a *CAG* promoter and the woodchuck hepatitis virus post-transcriptional regulatory element (*WPRE*)[9]. Using the same expression strategy, we created four new Cre-dependent mouse lines that express optogenetic tools: the H134R mutant of ChR2 (ref. 25) fused to either tdTomato (Ai27; ChR2(H134R)-tdTomato) or EYFP (Ai32; ChR2(H134R)-EYFP); a modified version of Arch (Ai35; ss-Arch-EGFP-ER2, abbreviated as Arch-ER2)[6]; or eNpHR3.0 (Ai39; eNpHR3.0-EYFP)[23] (**Fig. 1a**). ChR2(H134R) was chosen because it produces larger conductance changes than wild-type ChR2, likely owing to its slower deactivation kinetics. Both Arch-ER2 and eNpHR3.0 have Kir2.1 endoplasmic reticulum export signals that enhance proper expression of microbial opsin proteins to the cell membrane[6,21–23].

To examine Cre-dependent expression of the optogenetic reporters, we bred each line with *Emx1*-Cre mice. Consistent with *Emx1*-Cre's recombination pattern, all mice displayed strong native fluorescence throughout cortex and hippocampus (**Fig. 1b**). In each line, the fluorescent fusion proteins were primarily localized to the cell membrane with minimal accumulation in the cytoplasm. This was best seen in the cell body layer of all hippocampal subfields (CA1, CA3 and dentate gyrus), where the fluorescence was lower than in the dendritic layers and was ring shaped (**Fig. 1b**,**c**). Axon fibers extending from the cortex and hippocampus, as well as their termination zones (for example, thalamus), were also strongly labeled (**Fig. 1b**). Axon fiber fluorescence in *Emx1*-Cre;Ai39 mice appeared weaker than in other lines, indicating possible lower protein expression. We mapped the mRNA expression of the opsin fusion genes by *in situ* hybridization (ISH) on brain sections (**Fig. 1d**). All showed strong ISH signals in the cortex and hippocampus at the single-cell level, similar to expression seen in our Cre reporter mouse lines that express fluorescent proteins[9].

In the absence of Cre, we saw no leaky expression at the mRNA or fluorescence level in Ai27 and Ai32 mice, although we did see some leakage at the mRNA level in Ai35 and Ai39 mice (**Supplementary Figs. 1a** and **2a**). In addition to *Emx1*-Cre, strong Cre-dependent expression of opsin-fusion genes was also seen throughout the brain in other Cre-driver crosses (for example, *Pvalb*-IRES-Cre, *Camk2a*-CreERT2, *Chat*-IRES-Cre) (**Supplementary Figs. 1b**, **2b** and **3**), consistent with previous studies of our Cre-dependent fluorescent reporter mice[9]. In all cases, we saw plasma membrane targeting of all four transgenes, with no detectable intracellular protein aggregates, as shown in the *Pvalb*$^+$ interneurons in the cortex of the four types of *Pvalb*-IRES-Cre/reporter mice (**Supplementary Fig. 1b**). Long-term expression of these optogenetic transgenes in the various Cre-defined cell populations did not produce observable toxicity (**Supplementary Fig. 4**). The robust and widespread opsin-fusion expression observed in these multiple lines thus suggests that a variety of cell populations will be amenable to photomanipulation by these Cre-dependent optogenetic tools.

Effective light-activation of cortical pyramidal neurons

We investigated the photoexcitability of cortical pyramidal neurons from *Emx1*-Cre;Ai27 and *Emx1*-Cre;Ai32 mice (abbreviated as E-Ai27 and E-Ai32, respectively), and Ai32 alone mice not crossed to any Cre line (−Cre), by whole-cell recordings in the barrel cortex of acute brain slices using a previously established photostimulation protocol[26,27] (**Fig. 2a**), and compared them to neurons in which ChR2 was expressed by IUE. ChR2-expressing neurons showed normal resting membrane potentials (E-Ai27, −65.7 ± 1.4 mV, n = 14; E-Ai32, −65.4 ± 1.4 mV, n = 9; Ai32 (−Cre), −66.6 ± 2.2 mV, n = 9; IUE, −66.0 ± 2.4 mV, n = 6; mean ± s.e.m.). For each trial, a series of 1-ms pulses of constant-power blue light (473 nm) was applied through an air-immersion objective, sequentially in an 8 × 16 grid pattern overlaying cortical layers 1–5 (**Fig. 2a**). The grid covered the soma, dendrites and parts of the axonal arbor of the recorded layer 2/3 pyramidal neuron (**Fig. 2b**). In voltage clamp mode, modest laser powers evoked large photocurrents in E-Ai27 and E-Ai32 cells (**Fig. 2b**). With high laser powers (1,350–1,700 µW), spikes often accompanied the large photocurrents (peak current for E-Ai27, 1.51 ± 0.24 nA, n = 10; for E-Ai32: 2.01 ± 0.04 nA, n = 7). Even under high power stimulation conditions, no detectable photocurrent was recorded from Ai32 (−Cre) control cells (**Fig. 2b**, n = 9). In current clamp mode, action potentials were evoked in 12 of 14 E-Ai27 cells (2 cells showed subthreshold or no response); in 9 of 9 E-Ai32 cells, which is comparable to that of IUE cells[26,28]; and in 0 of 9 Ai32 (−Cre) cells (**Fig. 2c**,**d**).

To compare the photosensitivity, each cell was stimulated with a series of varying laser powers to determine the threshold for evoking an action potential (**Fig. 2e**). We found that E-Ai27 cells showed substantial heterogeneity in their thresholds for spiking, whereas E-Ai32 cells showed consistently low thresholds (**Fig. 2e**,**f**). The average threshold powers were, for E-Ai27, 919 ± 146 µW (range, 550–1,720 µW; n = 12); E-Ai32, 67 ± 6 µW (range, 55–116 µW; n = 9); and IUE, 56 ± 17 µW (range 8–128 µW; n = 7) (**Fig. 2e**). We further found that high power stimulation consistently evoked

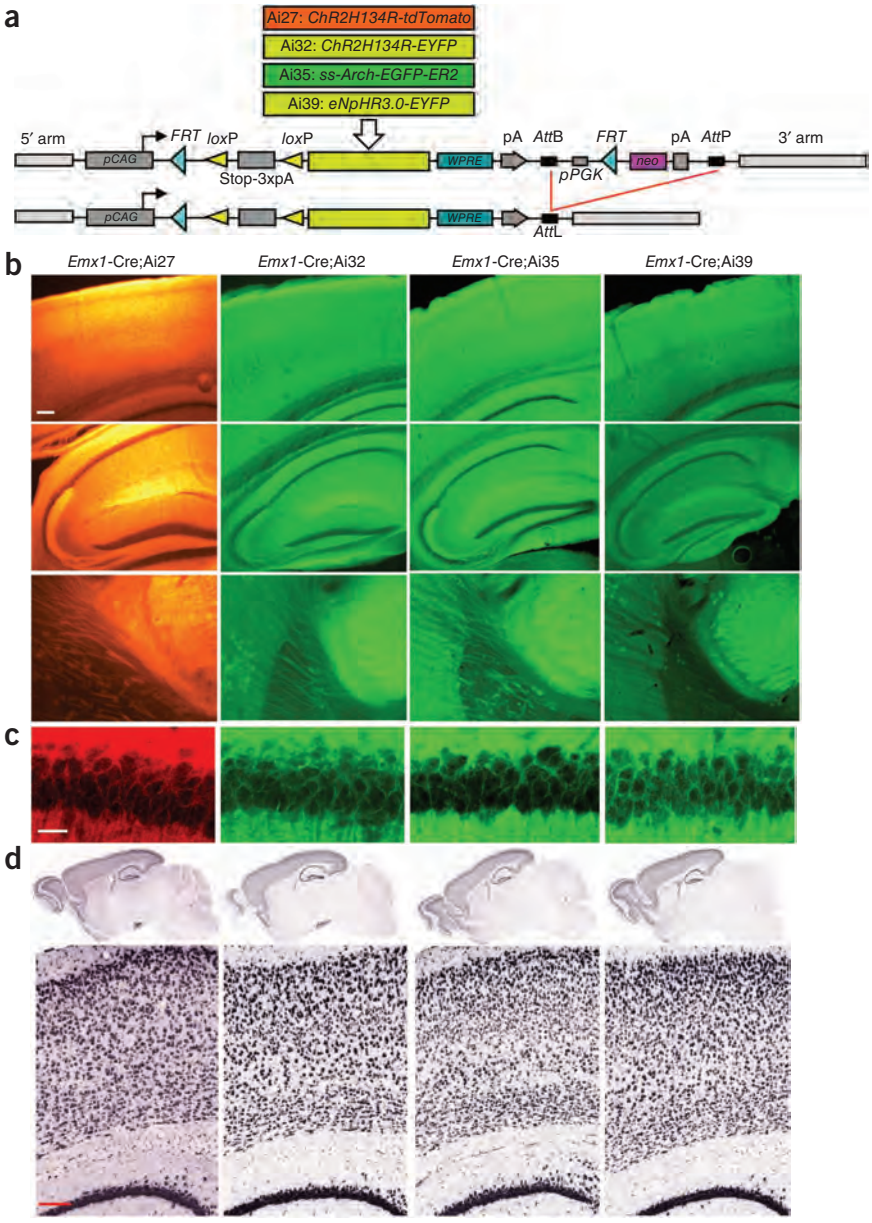

Figure 1 Generation and expression characterization of the Ai27, Ai32, Ai35 and Ai39 Cre-reporter lines. (**a**) Gene targeting vectors designed to insert the Cre-dependent reporter cassettes into intron 2 of the *Rosa26* locus. After obtaining germline-transmitted F_1 mice, the *pPGK-neo* selection cassette can be deleted by PhiC31-mediated recombination between the *Att*B and *Att*P sites, which combine into an *Att*L site, by breeding with a *Rosa26*-PhiC31 deleter line. pA, poly(A); pCAG, CAG promoter; pPGK, PGK promoter. (**b**) tdTomato, EYFP and EGFP native fluorescence in E-Ai27, E-Ai32, E-Ai35 and E-Ai39 mice. Scale bar, 200 µm. (**c**) Confocal images of the CA1 pyramidal neurons in the same mice as in **b**, showing the cell membrane localization of tdTomato, EYFP and EGFP fluorescence. Scale bar, 20 µm. (**d**) Reporter gene mRNA expression in E-Ai27, E-Ai32, E-Ai35 and E-Ai39 mice (ages all ~56 d), using *in situ* hybridization (Ai27, *tdTomato* riboprobe; Ai32, Ai35 and Ai39, riboprobe binding to EGFP/EYFP). Scale bar, 200 µm.

action potentials on more sites of the grid for E-Ai32 cells than for E-Ai27 cells (**Fig. 2g**) and with shorter spike latencies (**Fig. 2h**). Notably, low laser powers evoked action potentials in E-Ai32 cells similarly to IUE cells, but E-Ai32 cells showed less variability in the number of sites that could trigger an action potential (**Fig. 2i**).

Photoexcitation of axons is desirable for stimulating long-range postsynaptic neurons. The subcellular distribution of ChR2 will also influence the spatial resolution of photostimulation in brain slices and *in vivo*[29]. Antidromic action potentials triggered in axons can be distinguished from those triggered in the somata and dendrites because somatic or dendritic action potentials are associated with a slow charging phase preceding the action potential threshold, whereas axon-initiated action potentials arrive in the soma without previous charging[30] (**Fig. 2c**). By analyzing the charging phase, we categorized each action potential as originating from either somatic/dendritic or axonal stimulation (**Fig. 2d**). Under our photostimulation conditions, both E-Ai27 and E-Ai32 cells were preferentially excited in axons, whereas E-Ai32 cells, like IUE cells, were also more readily excited in the somata and dendrites than E-Ai27 (**Supplementary Fig. 5**). In sum, our results demonstrate that whereas E-Ai27 cells are less sensitive to photostimulation, the light response properties of E-Ai32 cells are comparable in many aspects to those of IUE ChR2-expressing cells.

Effective light-silencing of cortical pyramidal neurons

To test light-evoked neuronal silencing, we performed whole-cell recordings from layer 2/3 or layer 5 cortical pyramidal neurons (**Fig. 3a**) in acute slice preparations taken from adult *Emx1*-Cre;Ai35 or *Emx1*-Cre;Ai39 mice (abbreviated as E-Ai35 and E-Ai39, respectively). In all pyramidal neurons tested (29/29), illumination with a 200-µm optical fiber coupled to a 593-nm yellow laser caused marked hyperpolarization from the resting membrane potential. The response was very similar to that produced by a hyperpolarizing current injection before the light pulse (**Fig. 3b**). Recorded neurons exhibited a variety of responses to hyperpolarizing currents injected under current clamp conditions. Some exhibited hyperpolarization-activated I_h currents and/or rebound firing of action potentials in response to a transient application of a hyperpolarizing current, whereas others did not. In each case, the effect of the input current could be effectively reproduced by light (**Fig. 3b**). Upon repeated cycles of light stimulation (23 mW mm^{-2}), the extent of hyperpolarization diminished to about two-thirds the initial value, then reached a plateau in E-Ai39 cells (**Fig. 3c**). The E-Ai39 cells could recover from such diminished response to >90% original level after ~5 min rest between the cycles. Unlike E-Ai39 neurons, the responses in E-Ai35 neurons did not diminish with repeated light stimulation (**Fig. 3c**).

Both E-Ai35 and E-Ai39 cells showed larger hyperpolarization with increased light intensities (**Fig. 3d**). The mean maximal hyperpolarization (measured at 23 mW mm^{-2}) was 26.39 ± 2.67 mV for E-Ai35 (n = 15) and 12.96 ± 1.39 mV for E-Ai39 (n = 14). Under voltage clamp conditions, light-induced currents corresponded to light intensity and were highly reproducible from cell to cell (**Fig. 3e,f**). The photocurrents

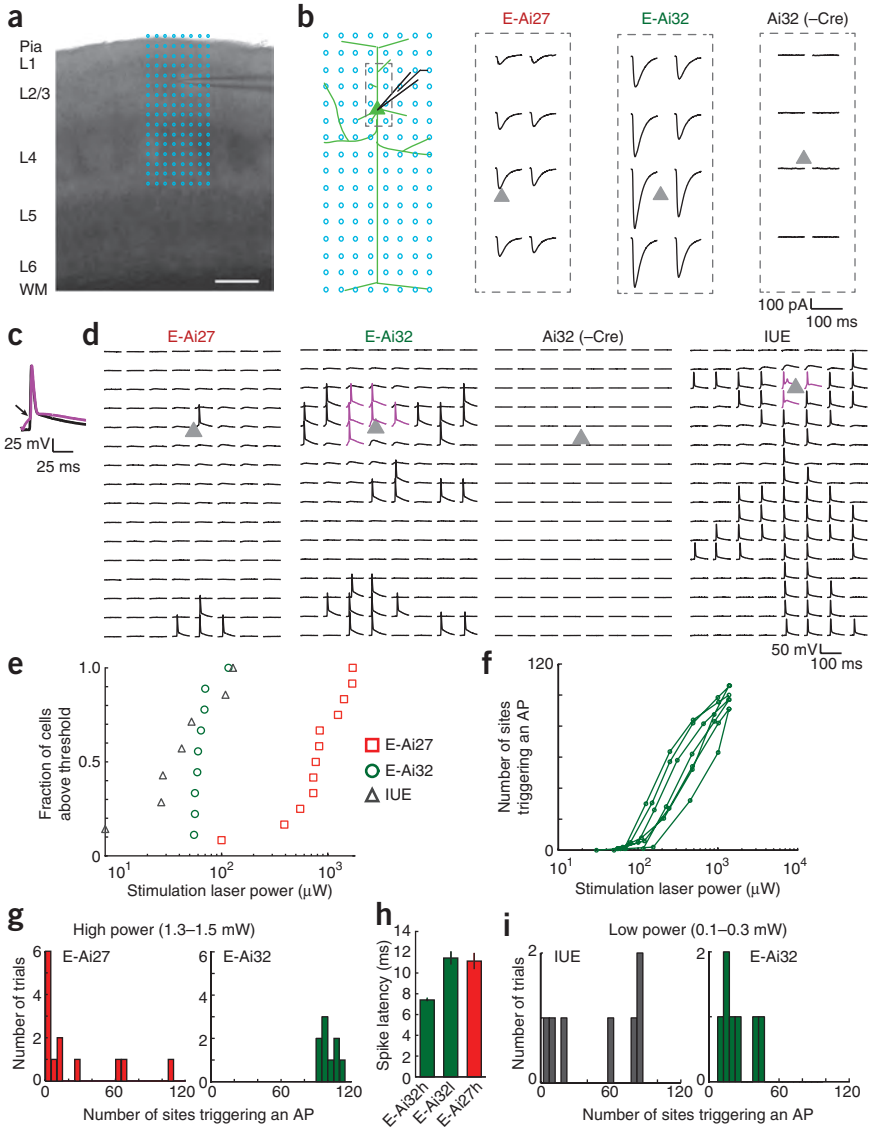

Figure 2 Photostimulation of pyramidal neurons in cortical slices of E-Ai27, E-Ai32 and Ai32 alone (–Cre) mice. (**a**) A barrel cortex slice with the 8 × 16 photostimulation grid overlaid (blue dots; spacing, 50 μm). Scale bar, 200 μm. L, layer. WM, white matter. (**b**) Schematic of the photostimulation geometry and example traces. Whole-cell voltage-clamp traces from the dashed box area (left) are shown for E-Ai27 (with 840 μW light), E-Ai32 (70 μW) and Ai32 (1,490 μW). Triangles, soma locations. (**c**) Waveforms of action potentials (APs) evoked by photoactivating the somata and dendrites (magenta) and axons (black). The arrow marks the inflection point. (**d**) Whole-cell current-clamp traces showing evoked APs in the 8 × 16 grid for a typical cell for each of E-Ai27 (1,700 μW), E-Ai32 (155 μW), Ai32 (1,500 μW) and IUE (155 μW). (**e**) Minimum laser power required to evoke an AP from at least one stimulation site. (**f**) Number of photostimulation sites evoking an AP as a function of laser power in E-Ai32 neurons ($n = 7$). (**g**) Number of stimulation sites triggering APs using high laser powers. (**h**) Spike latencies of somatic or dendritic APs from the light onset. E-Ai32h, E-Ai32 cells ($n = 9$ cells, 143 APs) under high powers (≥1 mW). E-Ai32l, E-Ai32 cells ($n = 9$ cells, 28 APs) under low powers (≤100 μW). E-Ai27, E-Ai27 cells ($n = 2$ cells, 4 APs) under high powers. (**i**) Number of stimulation sites triggering APs using low laser powers. Error bars, s.e.m.

attained in E-Ai35 neurons at low and high light levels were two to three times those observed in E-Ai39 neurons (1.7 mW mm^{-2}: $P < 0.05$, $n = 5$ for E-Ai35, $n = 7$ for E-Ai39; 23 mW mm^{-2}: $P < 0.01$, $n = 8$ for E-Ai35, $n = 9$ for E-Ai39) (**Fig. 3f**). Action potentials induced under current clamp by constant positive current injections were rapidly and reversibly inhibited by light illumination (23 mW mm^{-2}) in all trials in both E-Ai35 and E-Ai39 neurons (**Fig. 3g**). We conclude that Ai35-expressed Arch-ER2 is more efficient at generating photocurrents than Ai39-expressed eNpHR3.0, but that both transgenically expressed opsins are effective tools for the silencing of neural activity.

To ensure that no physiologically significant opsins were expressed from the uninduced reporter loci, we examined light-induced responses in cortical pyramidal neurons ($n = 4$) of Ai35 mice, as well as cortical ($n = 4$) and hippocampal CA1 ($n = 3$) pyramidal neurons of Ai39 mice, in the absence of any Cre allele. No light-induced changes were observed in the Ai35 (–Cre) cells at all, either at resting membrane potential (**Fig. 3h**,**i**) or when activated by a positive current injection (**Fig. 3j**), even with the highest intensity (23 mW mm^{-2}). Similarly, for Ai39 (–Cre) cells, light (593 nm, 23 mW mm^{-2}; or 640 nm, 24 mW mm^{-2}) caused no or negligible change in membrane potential (–0.02 ± 0.08 mV, $n = 7$, **Fig. 3i**). This is consistent with the leaky mRNA but absence of leaky protein expression in Ai39 (–Cre) mice (**Supplementary Figs. 1a** and **2**).

Silencing by alternative light sources

In addition to the yellow light (593 nm) that is near the excitation maximum of the Arch and NpHR proteins[4,6,31], we also tested neural silencing by two alternative light sources, a 640-nm red laser and a white LED, that offer several practical advantages. Red lasers are less expensive and more easily modulated than the yellow lasers. Though somewhat red-shifted relative to the excitation peaks of Arch and NpHR, longer wavelengths are also less prone to attenuation by light scattering, so the off-peak excitation may be partly offset by better tissue penetration. Red light also offers better spectral separation from the blue light used to activate ChR2, so it may be better suited for binary control of activity[4,32]. LEDs are inexpensive light sources and are potentially portable or implantable for experiments in moving animals.

These alternative light sources efficiently silenced both E-Ai35 and E-Ai39 cortical pyramidal neurons (**Fig. 4**). Both the LED and the 640-nm red laser produced an intensity-dependent drop in membrane potential (**Fig. 4b**,**e**,**g**,**i**) and effectively silenced current-induced spiking (**Fig. 4c**,**f**,**h**,**j**). At similar powers, the 640-nm light response of E-Ai35 neurons was 43 ± 5% (mean ± s.e.m.) of that obtained with 593-nm light (**Figs. 3d** and **4e**), and the 640-nm light response of E-Ai39 neurons was 100 ± 35% of that obtained with 593-nm light (**Figs. 3d** and **4i**), consistent with the red-shifted spectrum reported for eNpHR3.0 (ref. 23).

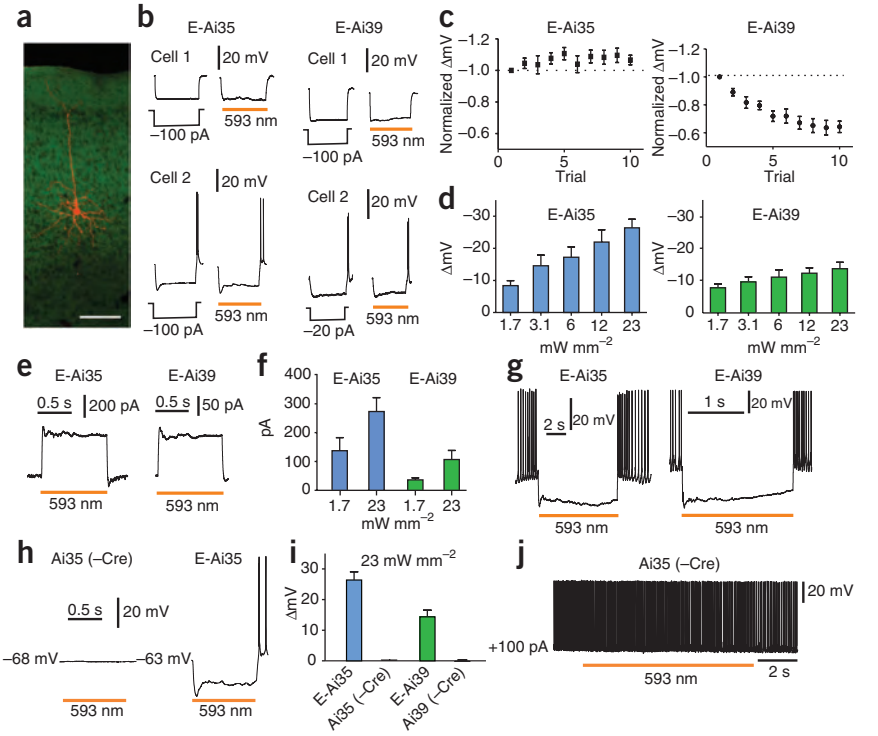

Figure 3 Effective silencing of cortical pyramidal neurons by Arch-ER2 in E-Ai35 and eNpHR3.0 in E-Ai39 mice. (**a**) Biocytin staining (red) of a cortical pyramidal neuron after recording. Scale bar, 100 µm. (**b**) Voltage responses of representative neurons to a 1-s negative current injection or a 1-s light pulse. Under both conditions, cell 2 from E-Ai35 and E-Ai39 exhibits rebound firing at the end of the stimulus, whereas cell 1 does not. (**c**) Voltage response of a neuron to ten consecutive trials of laser stimulation (1-s pulse, 1-s interpulse interval). Values are normalized to the first trial; first trial ΔV values were –27.05 ± 2.38 mV (E-Ai35, $n = 8$) and –19.43 ± 2.82 mV (E-Ai39, $n = 10$). (**d**) Average hyperpolarization from the resting membrane potential (mean of ten stimulations, as in **c**) evoked by different light intensities. (**e**) Representative photocurrent traces under voltage clamp (–70 mV) and 12 mW mm^{-2} illumination. (**f**) Mean photocurrents evoked by low and high light intensity. (**g**) Effective suppression of action potential firing in E-Ai35 or E-Ai39 neurons evoked by positive current injection (50–100 pA). (**h**) Voltage responses of Ai35 (–Cre) and E-Ai35 neurons under maximal light illumination (23 mW mm^{-2}). (**i**) Comparison of light-induced hyperpolarization in Cre-positive (E-Ai35, $n = 15$; E-Ai39, $n = 14$) and Cre-negative (Ai35, $n = 4$; Ai39, $n = 7$) neurons. (**j**) Maximum light (23 mW mm^{-2}) failed to slow or silence the firing of a Cre-negative Ai35 neuron evoked by positive current injection (100 pA). Error bars, s.e.m.

Light inhibition of hippocampal network activity

To test the effectiveness of E-Ai35 mice as a model for inhibiting neural network activity, we tested light-mediated silencing of a well described monosynaptic pathway from area CA3 to area CA1 of the hippocampus (**Fig. 5a**)[33]. In this model, we induced firing of hippocampal neurons in brain slice preparations by elevated K^+ and recorded population activity from CA1 (**Fig. 5b**). Focused illumination of the CA3 region produced an immediate drop in CA1 activity (**Fig. 5c**). With sustained illumination, CA3 firing increased, but it remained below baseline level. Partial release from silencing may occur over time because of compensatory effects in the network and/or because only a portion of the CA3 neurons with outputs to CA1 are inhibited by the focal illumination. After the light was turned off, firing rates returned quickly to baseline, and there was no rebound of spiking activity.

Dual recording from CA1 and CA3, combined with focal illumination of CA1, confirmed that these results were consistent with the silencing of a unidirectional synaptic input from CA3 to CA1 (**Fig. 5d,e**). First, illumination of CA1 had no effect on population activity in CA3. By contrast, direct illumination of CA1 caused immediate and nearly complete silencing of this region, and we observed a large rebound increase in firing on recovery from direct illumination of CA1. In addition, the extent of CA1 inhibition depended on

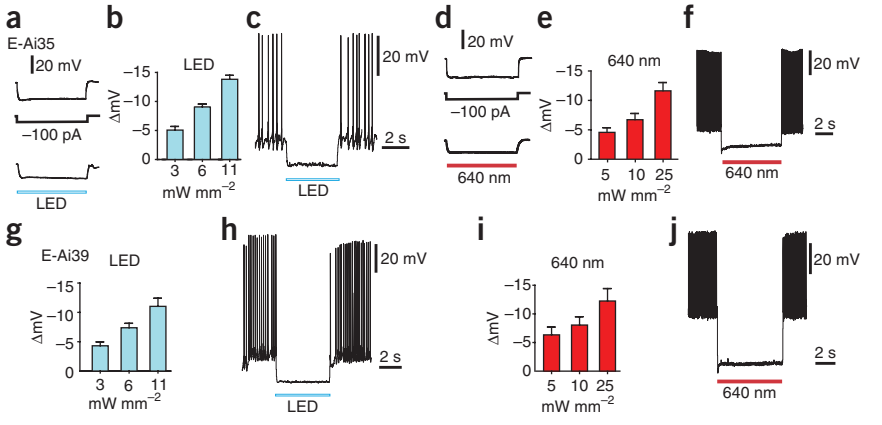

Figure 4 Alternative light sources for silencing of cortical pyramidal neurons in E-Ai35 and E-Ai39 mice. (**a**–**c**) Inhibition of E-Ai35 neurons by a white LED. (**a**) An example E-Ai35 neuron exhibited similar hyperpolarization responses to negative current injection (–100 pA) and illumination by white light. (**b**) White light dose-response curve ($n = 3$). (**c**) An example of effective silencing by white light (11 mW mm^{-2}) of action potentials evoked by a positive current injection (100 pA). (**d**–**f**) Inhibition of E-Ai35 neurons by red laser light (640 nm). (**d**) An example E-Ai35 neuron exhibited similar hyperpolarization responses to negative current injection (–100 pA) and illumination by red light. (**e**) Red light dose-response curve ($n = 7$). (**f**) An example of silencing of current-evoked action potentials by red laser light. (**g**,**h**) Inhibition of E-Ai39 neurons by a white LED. (**g**) White light dose-response curve ($n = 5$). (**h**) An example of silencing of current-evoked action potentials by white light. (**i**,**j**) Inhibition of E-Ai39 neurons by red laser light (640 nm). (**i**) Red light dose-response curve ($n = 7$). (**j**) An example of silencing of current-evoked action potentials by red laser light. Error bars, s.e.m.

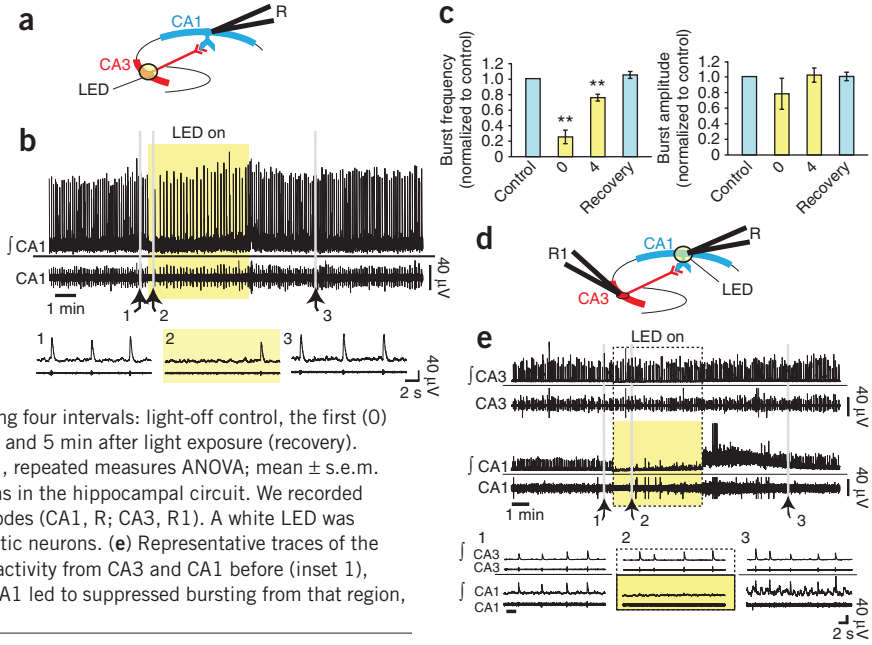

Figure 5 Effective silencing of induced population bursting in the hippocampal circuit in E-Ai35 mice. (**a**) Schematic for the inhibition of presynaptic neurons in the hippocampal circuit. We used an extracellular electrode (R) to record population bursting in CA1 induced by 8 mM K^+. A white light source (LED, yellow circle) was positioned over CA3 to activate Arch-ER2 in presynaptic neurons. (**b**) Representative traces of the integrated (top) and raw (bottom) population bursting activity from CA1 before (expanded traces in inset 1), during (2) and after (3) the illumination of CA3. Raw population bursting activity is the direct measure of unit activity. Integrated population activity represents the change of unit activity (time constant = 200 ms). (**c**) Quantified response of population bursting from CA1 ($n = 4$ experiments) during four intervals: light-off control, the first (0) and final (4) minute of a 5-min exposure to white light, and 5 min after light exposure (recovery). Values were normalized to light-off control. $^{**}P < 0.01$, repeated measures ANOVA; mean ± s.e.m. (**d**) Schematic for the inhibition of postsynaptic neurons in the hippocampal circuit. We recorded neurons simultaneously using dual extracellular electrodes (CA1, R; CA3, R1). A white LED was positioned over CA1 to activate Arch-ER2 in postsynaptic neurons. (**e**) Representative traces of the integrated (top) and raw (bottom) population bursting activity from CA3 and CA1 before (inset 1), during (2) and after (3) illumination of CA1. Light to CA1 led to suppressed bursting from that region, whereas bursting activity in CA3 was unaffected.

the area of illumination on CA3, under conditions of constant light intensity per unit area (**Supplementary Fig. 6**). We conclude that illumination of CA3 results in the selective inhibition of synaptic inputs to CA1, thus demonstrating the potential of Ai35 (and Ai39) mice for optogenetic studies of brain circuitry.

In vivo activation and silencing of cortical neurons

To evaluate the effectiveness of light modulation *in vivo* in these transgenic mouse lines, we performed extracellular recordings in awake, head-fixed adult mice. On the basis of a Monte Carlo simulation of light attenuation in brain tissues[6], we estimated light intensity at the electrode recording site to be 1–5% of that at the optical fiber tip, which was 500–900 μm above the recording site.

In E-Ai32 mice, we recorded a total of 16 units, including 7 single units and 9 multiple units. Of the 7 single units, firing rates increased in 6 units (**Fig. 6a**) and decreased in 1 unit, upon blue light (473 nm) illumination (0.8 mW from a 100-μm optical fiber, corresponding to ~100 mW mm^{-2} at the fiber tip and ~2 mW mm^{-2} at the recording sites). The light induced spiking was fast, reliable and precise after each pulse illumination (**Supplementary Fig. 7**). Precise activation was observed even when the fiber tip was 1.5–2.0 mm from the recording site, where light intensity is expected to drop to ~0.17% of that at the tip. Of the nine multiple units, firing rates increased in eight units and decreased in one unit. Light illumination and recording in an Ai32 (−Cre) mouse served as a negative control. Of the three cortical neurons recorded, none were modulated by light at the highest power. In E-Ai27 mice, we recorded a total of 11 units, including 4 single units and 7 multiple units. Of the 4 single units, firing rates significantly increased in only 1 unit and decreased in the other 3, with the same blue light illumination (2.2 mW, ~280 mW mm^{-2} at the 100-μm fiber tip and ~5 mW mm^{-2} at the recording sites). However, all 7 multiple units increased their firing rates. Overall, the single and multiple units with increased firing rates showed enhancements of 350–1,400% from the baseline for E-Ai32 (768 ± 94%, $n = 14$) and 150–350% for E-Ai27 (198 ± 25%, $n = 8$) (**Fig. 6b**). The magnitude of light-induced activation in E-Ai32 was significantly higher than that in E-Ai27, consistent with that observed *in vitro* (**Fig. 2**).

To evaluate the efficiency of optical silencing *in vivo* mediated by eNpHR3.0 and Arch-ER2 (**Fig. 6c**,**d**), we used E-Ai35, *Camk2a*-CreERT2;Ai35 and *Camk2a*-CreERT2;Ai39 mice. After tamoxifen induction, *Camk2a*-CreERT2 drives eNpHR3.0 or Arch-ER2 expression in most cortical pyramidal neurons similarly to *Emx1*-Cre (**Supplementary Fig. 1**)[9]. In an E-Ai35 mouse, we recorded a total of ten single units in cell-attached mode with glass electrodes. All single units significantly reduced their firing rates upon green light illumination (532 nm, 16 mW, ~470 mW mm^{-2} at the 200-μm fiber tip and ~13 mW mm^{-2} at the recording sites) (**Fig. 6c**). The recorded neurons showed a reduction of 83–100% from the baseline firing rates (93 ± 2%, $n = 10$) (**Fig. 6e**, left). Light-induced silencing was instantaneous, with 0 ms latency for nine of the ten neurons recorded. The population latency was 1 ± 1 ms from light onset (**Fig. 6e**, right). We observed similar results of complete silencing of single-unit activities in a tamoxifen-induced *Camk2a*-ERT2;Ai35 mouse (93 ± 7% silencing at ~10 mW mm^{-2} at the recording sites, $n = 2$). Light illumination and recording in an Ai35 (−Cre) mouse served as a negative control. Of the eight cortical neurons recorded, none were modulated by light at the highest power used (~16 mW mm^{-2} at the recording sites).

In a tamoxifen-induced *Camk2a*-CreERT2;Ai39 mouse, we recorded a total of 13 single units. Of these, 7 significantly reduced their firing rates (**Fig. 6d**), 3 did not change and 3 increased their firing rates upon green light illumination (11 mW, ~1,400 mW mm^{-2} at the 100-μm fiber tip and ~30 mW mm^{-2} at the recording sites). The single units with reduced firing rates showed a reduction of 83–97% from the baseline (90 ± 2%, $n = 7$), with 0–20 ms latency from light onset (8.6 ± 4.0 ms) (**Fig. 6e**). The magnitude of silencing in Ai39 mice with 30 mW mm^{-2} light was comparable to that observed in Ai35 mice with 10 mW mm^{-2} light ($P = 0.4$), but the latency of silencing in Ai39 mice was significantly longer than that in Ai35 mice ($P < 0.05$). The observed incomplete inhibition could result from the neurons that did not express *Camk2a*-CreERT2 and thus were disinhibited or activated through neural network mechanisms, consistent with previous observations using a viral labeling method *in vivo*[24].

We then compared the responses of the same single units to different light intensities. These single units in both E-Ai35 and

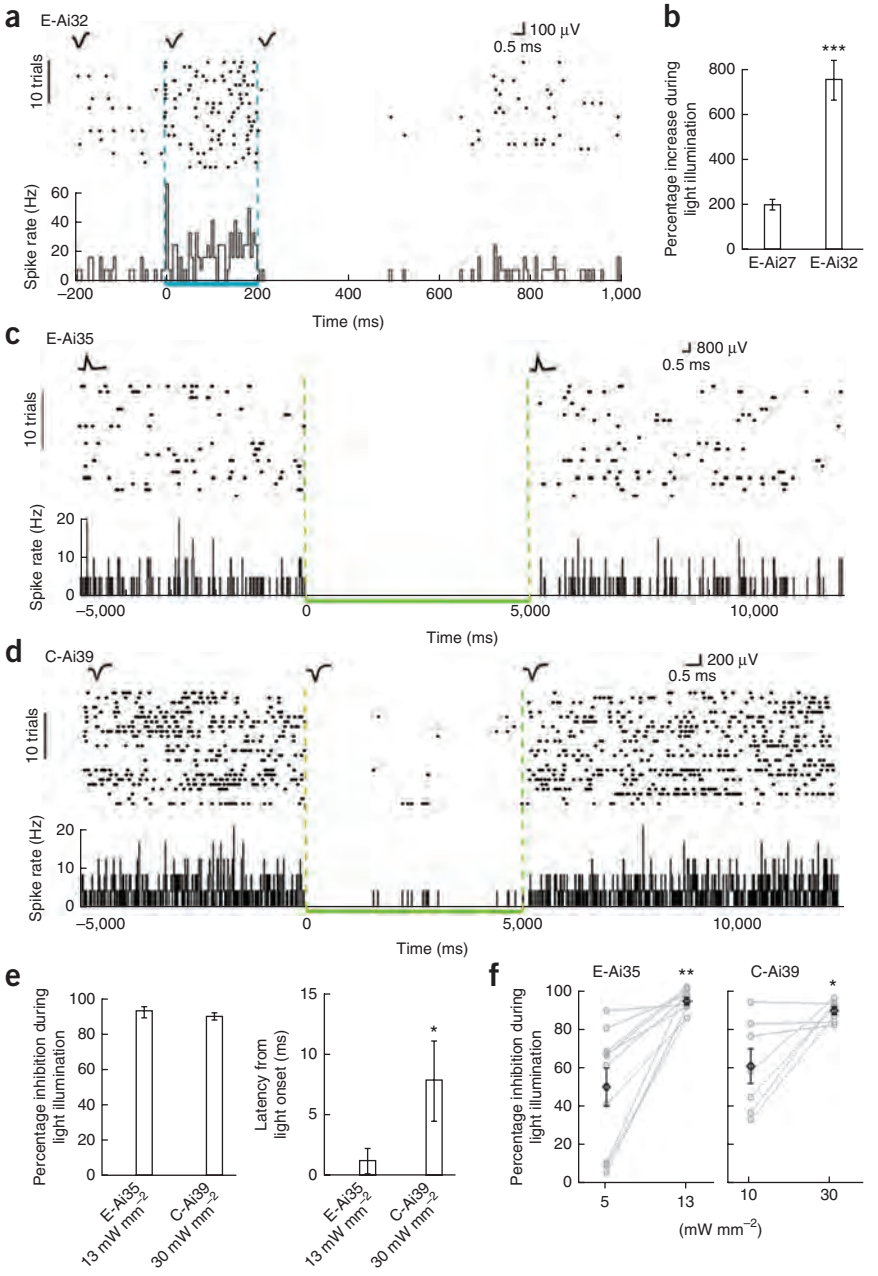

Figure 6 Optical activation or silencing of pyramidal neuron activities in the neocortex of awake E-Ai27, E-Ai32, E-Ai35 and *Camk2a*-CreERT2;Ai39 (C-Ai39) mice. (**a**) Neural activity and spike waveforms in a representative E-Ai32 neuron before, during and after 200-ms blue light illumination (3 mW mm^{-2}). Top, spike raster plot; bottom, histogram of instantaneous firing rate averaged across trials (bin size, 5 ms). (**b**) Average changes in firing rates upon blue light illumination in E-Ai27 and E-Ai32 mice. ***$P < 0.001$. (**c**) Neural activity and spike waveforms in a representative E-Ai35 neuron before, during and after 5-s green light illumination (13 mW mm^{-2}). (**d**) Neural activity and spike waveforms in a representative C-Ai39 neuron before, during and after 5-s green light illumination (30 mW mm^{-2}). In **c**,**d**, top, spike raster plot; bottom, histogram of instantaneous firing rate averaged across trials (bin size, 10 ms). (**e**) Average changes in firing rates (left) and latencies (right) observed in E-Ai35 and C-Ai39 single units during green light illumination at indicated light intensities. *$P < 0.05$. (**f**) Green light illumination at higher intensity induced more powerful silencing in E-Ai35 and C-Ai39 mice. *$P < 0.05$, **$P < 0.01$. All data are mean ± s.e.m.

Camk2a-CreERT2;Ai39 mice showed less inhibition at lower light intensities (**Fig. 6f**). In Ai35, firing rates were reduced by 49 ± 10% at 5 mW mm^{-2} and by 93 ± 2% at 13 mW mm^{-2} ($n = 10$, $P = 0.001$). In Ai39, firing rates were reduced by 62 ± 9% at 10 mW mm^{-2} and by 90 ± 2% at 30 mW mm^{-2} ($n = 7$, $P = 0.02$).

In vivo activation of *Pvalb*$^+$ interneurons

To examine photoexcitability in an inhibitory neuronal type, we performed extracellular recordings in awake, behaving *Pvalb*-IRES-Cre;Ai32 mice using a custom-designed optoelectronic probe[34] containing optical fibers 5–20 µm in diameter that deliver locally focused light (~1 mW at the tip). For an independent assessment of the specificity of *Pvalb*$^+$ neuron activation in these mice, we chose the hippocampal CA1 region and the thalamus because in these areas interneurons and principal cells can be reliably separated by physiological means[35–37]. In the hippocampus, the neuron with the typical autocorrelogram (ACG) of fast-firing perisomatic interneurons[38] was directly activated by both single pulses and a sinusoidal pattern (**Fig. 7a**). In contrast, the bursting, putative pyramidal cell was silenced at the time of the firing epoch of the activated neuron. Using previously established waveform criteria—trough-to-peak time and the width of the spike of the wide-band (1 Hz–5 kHz) unit at 20% of its peak amplitude[35,39]—we were able to segregate all recorded neurons into two main groups (**Fig. 7b** and **Supplementary Fig. 8**). All light activated neurons fell in the 'narrow-spike' category. In another comparison, we identified neurons as excitatory or inhibitory neurons on the basis of putative monosynaptic excitation and inhibition estimated by their short-time cross-correlograms[35,39,40]. Again, the two groups segregated and all activated neurons fell in the physiologically identified interneuron cluster (**Fig. 7b** and **Supplementary Fig. 8**). These results show that ChR2-mediated activation was absent in CA1 pyramidal cells and present in fast firing interneurons corresponding to the perisomatic *Pvalb*$^+$ interneurons.

In the thalamus, the characteristic low-threshold spike burst patterns of thalamocortical neurons can be reliably separated from those of the fast-firing inhibitory interneurons of the reticular nucleus[37]. In the mouse reticular nucleus, most interneurons are Pvalb immunoreactive[41]. Simultaneous recordings from reticular and the adjacent thalamocortical neurons and their local optogenetic activation generated two separate groups. Neurons that were activated by either single pulses or a sinusoidal pattern had ACGs characteristic of reticular neurons, whereas bursty neurons were suppressed by light stimulation (**Fig. 7c** and **Supplementary Fig. 9**). Light-activated and light-suppressed neurons had clearly different burst index magnitudes (**Fig. 7d**). These findings further support the specificity of

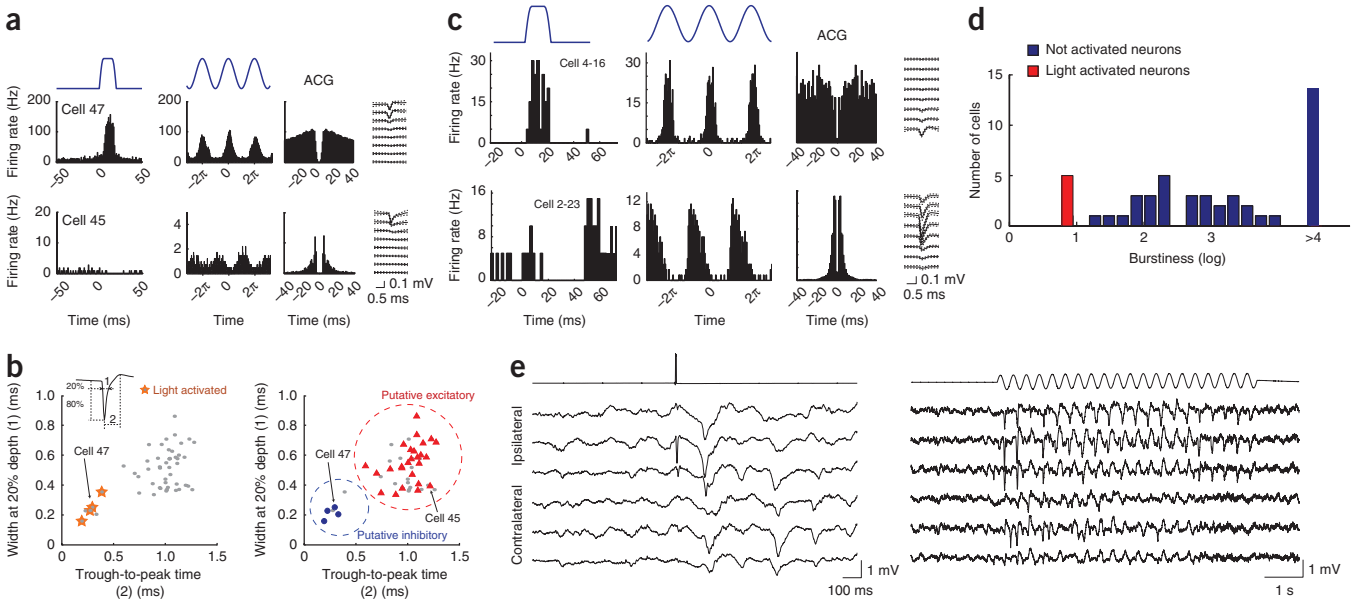

Figure 7 *In vivo* identification of light-activated neurons in the hippocampus and thalamus of *Pvalb*-IRES-Cre;Ai32 mice. (**a**) Excitation of ChR2-expressing neurons in the hippocampal CA1 region during the waking state. Top row of graphs shows peristimulus histogram of a *Pvalb*$^+$ neuron (cell 47) transiently activated by single pulses or 8-Hz, 1-mW sinusoidal light stimulation (top traces). Also shown are the autocorrelogram (ACG) and waveform (± s.e.m.) of the neuron (far right). Note typical ACG for a fast-firing putative basket cell[35]. Bottom row shows the same arrangement for a nearby pyramidal cell (cell 45). Note ACG typical of bursting neurons. (**b**) Optogenetic (left) and physiological (right) classifications of neuron types in the hippocampus. Physiological segregation of simultaneously recorded neurons is based on two parameters: (1) spike width and (2) trough-to-peak time (inset). (**c**) Activation of ChR2-expressing neurons in the thalamus during anesthesia. Top: a reticular nucleus *Pvalb*$^+$ neuron (cell 4-16) in response to single pulses or 10-Hz sinusoidal light stimulation. Bottom: a simultaneously recorded thalamocortical neuron (cell 2-23) with typical bursting pattern in ACG[36,37]. (**d**) Distribution of burst index in the activated (putative reticular, red) and suppressed (putative thalamocortical, blue) neurons. Burst index is the ratio of spikes with short (<6 ms) inter-spike intervals relative to other spikes in the same session. (**e**) Light-evoked cortical patterns in response to reticular nucleus stimulation in the waking *Pvalb*-IRES-Cre;Ai32 mice. Single-pulse (left) and sinusoidal pattern (10 Hz, right) evoked activities are epidural recordings from the ipsilateral and contralateral parietal areas.

ChR2-mediated activation in reticular *Pvalb*$^+$ interneurons. Although these physiological methods cannot distinguish between *Pvalb*$^+$ and other classes of interneurons[42], the physiological results are consistent with the previously demonstrated recombination specificity of *Pvalb*-IRES-Cre to *Pvalb*$^+$ interneurons in both hippocampus and thalamus[9].

As reticular inhibitory neurons are critical for pacing thalamocortical rhythm[37], we examined the effect of their light activation on neocortical activity of waking mice. Single pulse stimulation (5 ms, 20 mW) evoked a primary response, likely through rebound spike activation of thalamocortical neurons[36,37], followed by several cycles of activity typical of thalamocortical reverberation (**Fig. 7e**, left). Repetitive activation of reticular neurons at 10 Hz effectively entrained the thalamocortical circuit[36] (**Fig. 7e**, right). These findings demonstrate that reticular neurons can be recruited effectively by local light stimulation in *Pvalb*-IRES-Cre;Ai32 mice to induce physiologically relevant cortical patterns.

DISCUSSION

We have established four new transgenic mouse lines with robust Cre-dependent expression of ChR2, Arch-ER2 or eNpHR3.0. Compared to a previously published R26::ChR2-EGFP Cre-reporter mouse line[20], our Ai32 ChR2-EYFP–expressing line has substantially greater light sensitivity. In the R26::ChR2-EGFP mice, using very similar stimulation protocols in cortical slices, very long and strong laser pulses (~20 ms, ~2 mW) are needed to induce single spiking in interneurons, and even so spiking cannot be induced in pyramidal neurons. The mice also reportedly need a homozygous floxed ChR2 allele and dietary retinol. In contrast, the Ai32 mice possessed excitability with 1-ms light pulses at intensities as low as 30 µW, much larger photocurrents and much shorter latency to spiking, in pyramidal neurons. We further showed that pyramidal neurons and interneurons were readily excitable *in vivo* with low light in heterozygous mice. These improved properties are likely to prove critical in future *in vitro* and *in vivo* studies. Using such an efficient transgenic expression strategy is particularly essential for expressing the silencing opsins (Arch and eNpHR) to functional levels.

The transgenic targeting strategy used in the R26::ChR2-EGFP line[20] is similar to our strategy described here. Both targeted the *Rosa26* locus and used a strong and ubiquitous *CAG* promoter. But two main differences may be responsible for the improved expression in the new lines reported here. First, our expression cassettes included a *WPRE* sequence, which have previously been shown to enhance protein expression of *Rosa26*-targeted transgenes[9]. Second, while the R26::ChR2-EGFP line incorporated a commonly used floxed-stop cassette that contains the bacterial neomycin resistance (*neo*) gene in front of the stop, we intentionally excluded the *neo* gene from our own floxed-stop cassette and instead placed it separately downstream from the transgene expression cassette. Although it is unclear whether the relocation of the *neo* gene is helpful to the improved expression in our mice, it is well known that integration of bacterial sequences into mammalian genomes can cause epigenetic modifications that affect expression of nearby genes.

Each of our optogenetic lines exhibited distinct photo-response properties that could be useful for different applications. Neurons from Ai32 lines appeared significantly more photosensitive than those

from Ai27, both *in vitro* and *in vivo*. Although the basis for this difference between Ai27 and Ai32 neurons is unresolved, and we saw no apparent difference in expression level or membrane localization, we speculate that the bulkier tdTomato fluorescent tag in the Ai27 transgene may interfere with some channel properties. Although Ai32's photosensitivity seems desirable for most experiments, Ai27's red label and/or preferential axonal excitation may be advantageous in some applications[28,30]. Our *in vitro* and *in vivo* data on Ai35 and Ai39 neurons suggest that Arch-ER2 produces greater photocurrents and larger hyperpolarization than eNpHR3.0 under both green and yellow light. This could be due to the observed lower protein level for eNpHR3.0, even though the mice were generated using identical designs. However, owing to its broad and red-shifted activation spectrum, eNpHR3.0 is equally effective as Arch-ER2 under red light, and it may be preferable for dual-channel work together with blue light-responsive depolarizing opsins.

The kinetics of the *in vivo* light response of ChR2-expressing neurons in Ai27 and Ai32 mice were identical to those observed with virally expressed opsins, with a rapid increase in spiking at light onset, followed by stable, lower steady-state firing during light stimulation and often a period of suppression immediately after light termination[32]. Photoinhibition of Arch-ER2- or eNpHR3.0-expressing neurons in Ai35 or Ai39 mice *in vivo* yielded a near instantaneous reduction in firing rate, consistent with that observed with the viral infection method[6]. Many of the neurons recorded in Ai35 and Ai39 mice were nearly completely silenced. The homogenous and complete silencing in these mice represents an advantage over viral infection[6,24] of the consistent expression achieved in these transgenic mice.

An important question is the specificity of neuronal activity manipulation in the targeted populations. Although this can be addressed by exhaustive anatomical multiple labeling methods, physiological verification of specificity is also useful. We chose two brain areas, the CA1 pyramidal layer and the thalamus, because identification of principal cells and interneurons in these regions is possible by physiological means[35–40]. Although these methods cannot distinguish among the large family of interneurons[38], light-activated neurons displayed well known features of short-duration spikes and high firing rates typical of perisomatic *Pvalb*$^+$ interneurons. Conversely, putative CA1 pyramidal neurons and thalamocortical cells with bursting properties and excitatory connections were never directly activated by light. Instead, most of them were suppressed by light stimulation. These excellent physiological-optogenetic correlations in the intact brain support the cell type specificity of ChR2 activation. They also suggest that optogenetic activation of genetically labeled cell types, especially those difficult to distinguish by physiological or other means, will enable more refined *in vivo* identification and characterization of their functional properties[43].

Systematic expression characterization data from our previously generated fluorescent reporter lines (for example, Ai14), crossed to dozens of different Cre-driver lines, have shown that Cre-dependent activation of transgene expression can be obtained in nearly all neuronal types[9]. Thus, although data presented here are confined to the light responses of cortical and hippocampal pyramidal neurons and hippocampal and thalamic *Pvalb*$^+$ interneurons, we believe it highly likely that these optogenetic tools will effectively modulate activity in a wide range of neurons. It should be noted that different types of neurons may have different excitability properties for both intrinsic and/or local circuitry reasons and hence may require individual optimization of the conditions for activation and silencing.

Here we not only provide a new set of transgenic tools with superior properties for both stimulating and silencing neuronal activity, we also demonstrate a transgenic expression strategy having several conceptual advantages. First, because the opsins are expressed as single copies in an identical manner from a consistent genomic environment, reliable comparisons of *in vivo* performance can be made between different opsin genes and different transgenic lines. Second, the Cre-dependent on-off switch for transgene expression effectively prevents or minimizes leaky expression in nontargeted cells while enabling strong expression from the well characterized *CAG* promoter in targeted cells, an advantage over the specific promoter–driven single transgenic approach, in which the promoters used could have variable (sometimes unknown or uncharacterized) expression in both targeted and nontargeted cells. Third, because of the efforts we and others have taken to systematically characterize expression in Cre-driver lines[8,9], especially when similar reporter lines are used, documented and publicly available information about Cre recombination patterns (for example, http://connectivity.brain-map.org/transgenic/search/basic/) can advise researchers about the cell type specificity of expression expected when using a particular Cre driver with these reporter lines. This is of great importance also considering the potential for unintended ectopic Cre expression to varied degrees in some Cre lines and the need for informed choice about appropriate Cre (or inducible Cre) lines for specific cell types. Finally, this proven expression system will also facilitate the rapid incorporation of newly engineered optogenetic variants and, once validated, apply them to all the Cre lines. This presents a more 'one-for-all' opportunity than expressing one opsin in one cell type at a time, and it will further increase the range of optogenetic capabilities for investigating neural circuits and brain function.

METHODS

Methods and any associated references are available in the online version of the paper at http://www.nature.com/natureneuroscience/.

Accession codes, requests for materials and open data access. The four Cre-reporter mouse lines have been deposited with the Jackson Laboratory for distribution with stock numbers 012567 (Ai27), 012569 (Ai32), 012735 (Ai35) and 014539 (Ai39). The four gene-targeting DNA constructs (Ai27, Ai32, Ai35 and Ai39) have been deposited to Addgene for distribution. All ISH expression data are available at http://connectivity.brain-map.org/transgenic/search/basic.

Note: Supplementary information is available on the Nature Neuroscience website.

ACKNOWLEDGMENTS

We are grateful for the technical support of the Atlas Production Team, led by P. Wohnoutka, and the Technology Team, led by C. Dang, at the Allen Institute. We thank A. Nagy (Mount Sinai Hospital in Toronto) for providing the G4 ES cell line and K. Deisseroth (Stanford University) for providing the eNpHR3.0 construct. The authors wish to thank the Allen Institute founders, P.G. Allen and J. Allen, for their vision, encouragement and support. This work was funded by the Allen Institute for Brain Science and the Howard Hughes Medical Institute, US National Institutes of Health (NIH) grant DA028298 to H.Z., NIH grants MH90478 and MH093667 to E.E.T., NIH grant MH085944 and an Alfred P. Sloan Foundation grant to X.H., NIH grants NS034994 and MH54671 and a US National Science Foundation grant to G.B., and a Marie Curie Fellowship (EU FP7 PEOPLE 2009 IOF 254780) to A.B.

AUTHOR CONTRIBUTIONS

L.M., J.K. and H.G. generated the Cre reporter mouse lines. T.M., B.M.H. and K.S. conducted the slice physiology study on Ai27 and Ai32 mice. H.K., Y.-W.A.H., A.J.G., S.Z., J.M.R. and E.E.T. conducted the slice physiology study on Ai35 and Ai39 mice. J.Z., X.G., Y.M. and X.H. conducted the *in vivo* cortical recordings. A.B., S.F. and G.B. conducted the *in vivo* hippocampal and thalamic recordings. A.R.J. provided institutional support. E.S.B. provided the Arch-ER2 construct. L.M., T.M., H.K., J.Z., A.B., S.F., E.S.B., G.B., X.H., E.E.T. and H.Z. analyzed data and wrote the paper.

COMPETING FINANCIAL INTERESTS
The authors declare no competing financial interests.

Published online at http://www.nature.com/natureneuroscience/.
Reprints and permissions information is available online at http://www.nature.com/reprints/index.html.

1. Boyden, E.S., Zhang, F., Bamberg, E., Nagel, G. & Deisseroth, K. Millisecond-timescale, genetically targeted optical control of neural activity. *Nat. Neurosci.* **8**, 1263–1268 (2005).
2. Li, X. *et al.* Fast noninvasive activation and inhibition of neural and network activity by vertebrate rhodopsin and green algae channelrhodopsin. *Proc. Natl. Acad. Sci. USA* **102**, 17816–17821 (2005).
3. Nagel, G. *et al.* Channelrhodopsin-2, a directly light-gated cation-selective membrane channel. *Proc. Natl. Acad. Sci. USA* **100**, 13940–13945 (2003).
4. Han, X. & Boyden, E.S. Multiple-color optical activation, silencing, and desynchronization of neural activity, with single-spike temporal resolution. *PLoS ONE* **2**, e299 (2007).
5. Zhang, F., Aravanis, A.M., Adamantidis, A., de Lecea, L. & Deisseroth, K. Circuit-breakers: optical technologies for probing neural signals and systems. *Nat. Rev. Neurosci.* **8**, 577–581 (2007).
6. Chow, B.Y. *et al.* High-performance genetically targetable optical neural silencing by light-driven proton pumps. *Nature* **463**, 98–102 (2010).
7. Hegemann, P. & Moglich, A. Channelrhodopsin engineering and exploration of new optogenetic tools. *Nat. Methods* **8**, 39–42 (2011).
8. Gong, S. *et al.* Targeting Cre recombinase to specific neuron populations with bacterial artificial chromosome constructs. *J. Neurosci.* **27**, 9817–9823 (2007).
9. Madisen, L. *et al.* A robust and high-throughput Cre reporting and characterization system for the whole mouse brain. *Nat. Neurosci.* **13**, 133–140 (2010).
10. Taniguchi, H. *et al.* A resource of Cre driver lines for genetic targeting of GABAergic neurons in cerebral cortex. *Neuron* **71**, 995–1013 (2011).
11. Atasoy, D., Aponte, Y., Su, H.H. & Sternson, S.M.A. FLEX switch targets Channelrhodopsin-2 to multiple cell types for imaging and long-range circuit mapping. *J. Neurosci.* **28**, 7025–7030 (2008).
12. Kuhlman, S.J. & Huang, Z.J. High-resolution labeling and functional manipulation of specific neuron types in mouse brain by Cre-activated viral gene expression. *PLoS ONE* **3**, e2005 (2008).
13. Arenkiel, B.R. *et al. In vivo* light-induced activation of neural circuitry in transgenic mice expressing channelrhodopsin-2. *Neuron* **54**, 205–218 (2007).
14. Wang, H. *et al.* High-speed mapping of synaptic connectivity using photostimulation in Channelrhodopsin-2 transgenic mice. *Proc. Natl. Acad. Sci. USA* **104**, 8143–8148 (2007).
15. Hägglund, M., Borgius, L., Dougherty, K.J. & Kiehn, O. Activation of groups of excitatory neurons in the mammalian spinal cord or hindbrain evokes locomotion. *Nat. Neurosci.* **13**, 246–252 (2010).
16. Chuhma, N., Tanaka, K.F., Hen, R. & Rayport, S. Functional connectome of the striatal medium spiny neuron. *J. Neurosci.* **31**, 1183–1192 (2011).
17. Ren, J. *et al.* Habenula "cholinergic" neurons co-release glutamate and acetylcholine and activate postsynaptic neurons via distinct transmission modes. *Neuron* **69**, 445–452 (2011).
18. Tsunematsu, T. *et al.* Acute optogenetic silencing of orexin/hypocretin neurons induces slow-wave sleep in mice. *J. Neurosci.* **31**, 10529–10539 (2011).
19. Zhao, S. *et al.* Cell type–specific channelrhodopsin-2 transgenic mice for optogenetic dissection of neural circuitry function. *Nat. Methods* **8**, 745–752 (2011).
20. Kätzel, D., Zemelman, B.V., Buetfering, C., Wolfel, M. & Miesenbock, G. The columnar and laminar organization of inhibitory connections to neocortical excitatory cells. *Nat. Neurosci.* **14**, 100–107 (2011).
21. Zhao, S. *et al.* Improved expression of halorhodopsin for light-induced silencing of neuronal activity. *Brain Cell Biol.* **36**, 141–154 (2008).
22. Gradinaru, V., Thompson, K.R. & Deisseroth, K. eNpHR: a *Natronomonas* halorhodopsin enhanced for optogenetic applications. *Brain Cell Biol.* **36**, 129–139 (2008).
23. Gradinaru, V. *et al.* Molecular and cellular approaches for diversifying and extending optogenetics. *Cell* **141**, 154–165 (2010).
24. Han, X. *et al.* A high-light sensitivity optical neural silencer: development and application to optogenetic control of non-human primate cortex. *Front. Syst. Neurosci.* **5**, 18 (2011).
25. Nagel, G. *et al.* Light activation of channelrhodopsin-2 in excitable cells of *Caenorhabditis elegans* triggers rapid behavioral responses. *Curr. Biol.* **15**, 2279–2284 (2005).
26. Petreanu, L., Huber, D., Sobczyk, A. & Svoboda, K. Channelrhodopsin-2-assisted circuit mapping of long-range callosal projections. *Nat. Neurosci.* **10**, 663–668 (2007).
27. Petreanu, L., Mao, T., Sternson, S.M. & Svoboda, K. The subcellular organization of neocortical excitatory connections. *Nature* **457**, 1142–1145 (2009).
28. Lewis, T.L. Jr., Mao, T. & Arnold, D.B. A role for myosin VI in the localization of axonal proteins. *PLoS Biol.* **9**, e1001021 (2011).
29. Peron, S. & Svoboda, K. From cudgel to scalpel: toward precise neural control with optogenetics. *Nat. Methods* **8**, 30–34 (2011).
30. Lewis, T.L. Jr., Mao, T., Svoboda, K. & Arnold, D.B. Myosin-dependent targeting of transmembrane proteins to neuronal dendrites. *Nat. Neurosci.* **12**, 568–576 (2009).
31. Zhang, F. *et al.* Multimodal fast optical interrogation of neural circuitry. *Nature* **446**, 633–639 (2007).
32. Han, X. *et al.* Millisecond-timescale optical control of neural dynamics in the nonhuman primate brain. *Neuron* **62**, 191–198 (2009).
33. Ishizuka, N., Weber, J. & Amaral, D.G. Organization of intrahippocampal projections originating from CA3 pyramidal cells in the rat. *J. Comp. Neurol.* **295**, 580–623 (1990).
34. Royer, S. *et al.* Multi-array silicon probes with integrated optical fibers: light-assisted perturbation and recording of local neural circuits in the behaving animal. *Eur. J. Neurosci.* **31**, 2279–2291 (2010).
35. Csicsvari, J., Hirase, H., Czurkó, A., Mamiya, A. & Buzsáki, G. Oscillatory coupling of hippocampal pyramidal cells and interneurons in the behaving rat. *J. Neurosci.* **19**, 274–287 (1999).
36. Halassa, M.M. *et al.* Selective optical drive of thalamic reticular nucleus generates thalamic bursts and cortical spindles. *Nat. Neurosci.* **14**, 1118–1120 (2011).
37. Steriade, M., McCormick, D.A. & Sejnowski, T.J. Thalamocortical oscillations in the sleeping and aroused brain. *Science* **262**, 679–685 (1993).
38. Klausberger, T. *et al.* Brain-state- and cell-type-specific firing of hippocampal interneurons *in vivo*. *Nature* **421**, 844–848 (2003).
39. Sirota, A. *et al.* Entrainment of neocortical neurons and gamma oscillations by the hippocampal theta rhythm. *Neuron* **60**, 683–697 (2008).
40. Fujisawa, S., Amarasingham, A., Harrison, M.T. & Buzsaki, G. Behavior-dependent short-term assembly dynamics in the medial prefrontal cortex. *Nat. Neurosci.* **11**, 823–833 (2008).
41. Liu, X.B., Murray, K.D. & Jones, E.G. Low-threshold calcium channel subunit Ca_v 3.3 is specifically localized in GABAergic neurons of rodent thalamus and cerebral cortex. *J. Comp. Neurol.* **519**, 1181–1195 (2011).
42. Tanahira, C. *et al.* Parvalbumin neurons in the forebrain as revealed by parvalbumin-Cre transgenic mice. *Neurosci. Res.* **63**, 213–223 (2009).
43. Lima, S.Q., Hromadka, T., Znamenskiy, P. & Zador, A.M. PINP: a new method of tagging neuronal populations for identification during *in vivo* electrophysiological recording. *PLoS ONE* **4**, e6099 (2009).

ONLINE METHODS

Animal procedures. All experimental procedures related to the use of mice were approved by the Institutional Animal Care and Use Committees of the Allen Institute for Brain Science, the Howard Hughes Medical Institute, Boston University, Seattle Children's Research Institute, or Rutgers University, in accordance with NIH guidelines. A total of ~70 mice, both male and female, were used in the study.

Gene targeting in ES cells and generation of knock-in Cre reporter mice. Targeting constructs were generated using a combined gene synthesis (GenScript) and molecular cloning approach. ChR2(H134R)-tdTomato was synthesized based on the hChR2 sequence[26], and ChR2(H134R)-EYFP was synthesized based on the ChR2 sequence[3]. Both fragments, as well as the ss-Arch-EGFP-ER2 (ref. 6) and the eNpHR3.0-EYFP (ref. 23) fragments, were each cloned into a *Rosa26*-pCAG-LSL-WPRE-bGHpA targeting vector[9], between LSL and WPRE sequences. LSL sequence contains specifically *lox*P – Stop codons – 3x SV40 polyA – *lox*P.

The targeting vectors were linearized and transfected into the 129/B6 F1 hybrid ES cell line G4 (ref. 44). G418-resistant ES clones were first screened by PCR using primers spanning the 1.1 kb 5′ genomic arm (forward primer: 5′-gggctccg gctcctcagaga-3′, reverse primer: 5′-atgccaggcgggccatttac-3′), and then confirmed by Southern blot analysis of HindIII-digested DNA, which was probed with a 1.1 kb genomic fragment from immediately upstream of the 5′ arm. Positive ES clones were injected into C57BL/6J blastocysts to obtain chimeric mice following standard procedures. Chimeric mice were bred with C57BL/6J mice to obtain germline transmitted F1 mice. The reporter mice can be bred with the *Rosa26*-PhiC31 mice (JAX stock # 007743)[45] to delete the PGK-neo cassette in the germline of the mice.

Expression characterization. Reporter mice were crossed to various Cre lines, including *Emx1*-Cre (JAX stock # 005628), *Camk2a*-CreERT2 (JAX # 012362), *Pvalb*-IRES-Cre (JAX # 008069) and *Chat*-IRES-Cre (JAX # 006410). Expression of the reporter genes was assessed by both native fluorescence (without antibody staining) on perfused, microtomed sections and by ISH.

For ISH, the Allen Institute–established pipelines for tissue processing, probe hybridization, image acquisition and data processing were used. The procedures were previously described[9,46] and can be found at the Transgenic Mouse database (http://help.brain-map.org/display/mouseconnectivity/documentation/). Expression levels were analyzed with 2-tailed, paired or unpaired Student's *t*-test at an alpha level of 0.05.

Electrophysiology and photostimulation on Ai27 and Ai32 brain slices. P30–P60 mice were used. Recordings on 300-µm-thick barrel cortical slices were performed in the presence of 5 µM (R)-CPP (Tocris) and 10 µM NBQX (Tocris). Electrophysiology and stimulus conditions were as described[26]. A series of 473-nm laser pulses (Crystal Laser) of 1-ms duration and 30–1,770 µW (at specimen) for photostimulation was delivered through an air objective (4x; 0.16 NA; UPlanApo, Olympus) with a beam diameter of 6–20 µm (scattering in the tissue was not taken into account). Photostimulation marched through an 8 × 16 grid with 50 µm spacing. The laser stimuli were given in a spatial sequence designed to avoid consecutive stimulation to neighboring spots to minimize desensitization[47]. Data were acquired using Ephus (http://www.ephus.org/).

Inflection point analysis. APs triggered in axons could be distinguished from those triggered in somata and dendrites by their waveforms. Dendritic APs have a charging phase that precedes reaching the AP threshold (set to be 15 mV) at the inflection points. To determine the charging phase and the inflection point, we calculated the first derivative of an AP trace. The AP was identified as a derivative peak larger than 25 mV/ms, the charging phase as a derivative peak before AP and larger than 0.5 mV/ms, and the inflection point as the lowest derivative point between the charging peak and the AP peak. APs with an inflection point higher than 15mV were scored as somatic/dendritic; otherwise, as axonal.

***In utero* electroporation.** *In utero* electroporation (IUE) was done as previously described[26,28]. In brief, the plasmids for electroporation contained ChR2-mVenus (2 µg/µl) and cytoplasmic mCherry at 3:1 molar ratio. E16 timed-pregnant C57BL/6J mice were deeply anesthetized using an isoflurane-oxygen mixture. The uterine horns were exposed and 0.2–0.5 µl of DNA solution with Fast Green dye (Sigma) was pressure injected (Picospritzer, General Valve) through a pulled glass capillary tube (Warner Instruments). The head of each embryo was placed between custom-made tweezer-electrodes, with the positive plate contacting the right side of the head. For E16 animals, the transfection was restricted to layer 2/3 cortical cells in the electroporated hemisphere. IUE mice were used for slice physiology at ages of P14–P21.

Electrophysiology and photostimulation on Ai35 and Ai39 brain slices. Mice 7–21 weeks old were used to prepare coronal slices (neocortex experiments, 350–400 µm thick; hippocampus experiments, 400–500 µm thick) for intracellular whole cell recordings. Illumination of brain slice preparations was supplied by a 593-nm, 50-mW yellow laser (LaserSight Technologies), a 640-nm, 50-mW diode red laser (Opto Engine) or a Luxeon 5 W white LED (Lumileds Lighting). Light sources were coupled to a 200-µm, 0.22-NA optical fiber. Light output was calibrated with a Thorlabs PM100 m and S130A detector (Thorlabs).

Hippocampal network recordings. Young adult mice (P35–50, **Fig. 5**) and adult mice (6 months, **Supplementary Fig. 6**) were used. Extracellular KCl was elevated from 3 to 8 mM over a 20-min period to initiate spontaneous bursting in the hippocampal slice. Experiments began 10 min after KCl reached 8 mM. Extracellular recordings were made from areas CA1 and CA3 using glass electrodes filled with ACSF (<2 MΩ). An optical fiber (200-µm diameter) connected to a computer-driven white LED source (**Fig. 5**) or a 640-nm laser (**Supplementary Fig. 6**) was positioned over CA3 or CA1. Population bursting and the integration of population bursts were recorded before, during and after the light stimulation. Integration of the population bursts was conducted in real-time using an in-line integrator (time constant = 200 ms; James Franck Institute electronic shop). Instantaneous frequency and amplitude of integrated bursts were analyzed *post hoc* using Clampfit 10. Differences were determined using 2-tailed unpaired *t*-test between two means, or one-way repeated measures ANOVA followed by multiple comparisons testing (Dunnett's comparison) among three or more means.

***In vivo* photostimulation and extracellular recording in awake, head-fixed mice.** Recordings in awake head-fixed mice (3–7 months old) were performed as previously described[6,32]. Briefly, under isoflurane anesthesia, a plastic head-plate was implanted over the cortex. Once the mouse recovered from surgery, recordings were made while the mouse was awake and head fixed, using linear multi-contact silicone electrodes (NeuroNexus). To avoid light-induced artifact on the silicone electrodes, we also used borosilicate glass microelectrodes filled with saline. The glass microelectrodes had an impedance of ~7 MΩ . Optical fibers were coupled to the electrodes (100-µm fiber coupled to silicone electrode, and 200-µm fiber to glass electrode), with the tip positioned 500–900 µm above the recording sites. The optical fiber was connected to a green laser (532 nm) or a blue laser (473 nm), with tunable power (Shanghai Laser Corp). Lasers were controlled by a function generator (Agilent Tech). Light intensity was measured with a power meter PM100D (Thorlabs). Data acquisition was performed with a multichannel Omniplex system (Plexon) for the NeuroNexus silicone electrode, or with a Multiclamp 700B amplifier and digitized with a Digidata 1440 digitizer (Molecular Device).

Spikes were sorted with Offline Sorter 3.0 (Plexon). Neurons modulated by light were identified by performing a paired *t*-test, for each neuron, between the baseline firing rate before light onset and firing rate during light illumination, across all trials for that neuron, thresholding at $P < 0.05$ significance level as previously described[6,32]. Instantaneous firing rate histograms were computed by averaging the instantaneous firing rate with a time bin of 10 ms for Ai35 and Ai39 neurons or 5 ms for Ai32 and Ai27 neurons.

Both green and blue light illumination of the silicone multi-contact electrodes produced significant slow artifacts, as previously observed with tungsten electrodes[32]. The blue light-induced artifact was particularly strong on the silicone electrodes, which sometimes saturated the data acquisition amplifier at the onset of each light pulse; thus, we excluded the first 20 ms after light onset for calculations for all Ai27 and Ai32 neurons. The green light-induced artifact on silicone electrodes was much smaller in magnitude, and never saturated the amplifier system, allowing us to determine the latency of light-induced neural modulation in Ai35 and Ai39 mice. Light did not produce any optical artifact on glass electrodes. Latency was defined as the time from light onset to the time at which firing rate was significantly different from baseline for the following 30 ms.

***In vivo* photostimulation and extracellular recording in behaving *Pvalb*-IRES-Cre;Ai32 mice.** Fiber-based optoelectronic probes were constructed as previously described[34]. The silicon probes have four shanks (Buzsaki32 from NeuroNexus). The shanks are 200 μm apart from each other and bear eight recording sites each (160 μm^2 each site; 1–3 MΩ impedance) arranged in a staggered configuration (20 μm vertical separation)[40]. As light guides, we used multi-mode optical fibers (105 μm in diameter; AFS 105/125; Thorlabs). To restrict light activation only to the brain volume monitored by the silicon probe, the fiber was etched by dipping into concentrated hydrofluoric acid until the desired 5–20 μm diameter was achieved. The fiber was positioned on the silicon shank ~100 μm above the uppermost recording site, and the rest of the fiber was glued to the shank. Light modulation was provided by DPSS laser (473 nm; SDL-473-050T; Shanghai Dream Lasers Technology). The intensity of light at the tip of the etched fiber could be varied. Typical stimulus intensity varied between 1 to 5 mW.

Recordings were performed either in anesthetized (isoflurane) or waking, freely behaving mice (6–8 weeks old). In the chronic mice, the optoelectronic probe assembly was fixed to a micromanipulator and lowered into the brain by slow steps. In mice with light activation of the reticular nucleus, etched optic fibers were placed in the reticular nucleus unilaterally or bilaterally. Cortical activity was monitored by epidural recordings, using no. 000 screws driven into the bone. Recording sessions typically lasted for 1 h, during which the animal's behavior alternated between periods of walking and immobility. Neurophysiological signals were amplified and multiplexed by a miniature head-stage of a 256-channel multiplexed amplifier system and the multiplexed signals were directly recorded by the computer. After recovery, the animals could move relatively unconstrained due to the low weight and small size of the head-stage as well as the low number of connecting wires. Neuronal activity was sampled at 20 kHz per channel at 16 bit resolution, while the overall gain of the multiplexer system was 400× (KJE-1000; Amplipex). Spike sorting was performed semi-automatically, using KlustaKwik, followed by manual adjustment of the clusters[48].

Considerations for light intensity measurement in different experimental paradigms. The amount of depolarization or hyperpolarization generated in a given cell is corresponding to the summation of the photocurrents generated from all the activated opsin molecules. The latter is proportional to irradiance (light intensity per unit area) at the target multiplied by the illuminated surface area of the target cell (including cell body and dendritic/axonal processes, without considering further heterogeneity in opsin distribution and local membrane excitability). Therefore illumination by a diffused light (for example, directly from a LED or through a regular optical fiber) with lower irradiance but covering a larger surface area of the cell could have the same effect as illumination by a high intensity and highly focused, therefore high irradiance, light beam (for example, laser light through the objective lens) on a smaller surface area of the cell. Furthermore, even highly focused light becomes scattered as it enters the brain tissue, and it is impossible to estimate the actual irradiance at the target without knowing the location and depth of the cell or which part of it is illuminated. For these reasons, different methods were employed to report the light intensities in our study. In brain slice photosilencing experiments (**Figs. 3**–**5**), irradiance (in mW mm^{-2}) of the relatively diffused light at the surface of the brain slice was presented. In brain slice photoactivation experiments (**Fig. 2**) radiant flux (that is, light intensity, in mW) of the focused light beam (6–20 μm wide) at the surface of the brain slice was presented. In the *in vivo* photostimulation of cortical excitatory neurons (**Fig. 6**), the irradiance at the recorded cell level was estimated by Monte Carlo simulation based on known distance between the tip of the optical fiber (100–200 μm wide) and the electrode. In the *in vivo* photostimulation of hippocampal and thalamic *Pvalb*-positive neurons (**Fig. 7**), radiant flux at the tip of the etched optical fiber (5–20 μm wide) that was attached to the silicon probe was reported. All these types of descriptions can be considered appropriate for cross-experimental comparisons in each of their respective protocols where the light delivery approach is consistent.

44. George, S.H. *et al.* Developmental and adult phenotyping directly from mutant embryonic stem cells. *Proc. Natl. Acad. Sci. USA* **104**, 4455–4460 (2007).
45. Raymond, C.S. & Soriano, P. High-efficiency FLP and PhiC31 site-specific recombination in mammalian cells. *PLoS ONE* **2**, e162 (2007).
46. Lein, E.S. *et al.* Genome-wide atlas of gene expression in the adult mouse brain. *Nature* **445**, 168–176 (2007).
47. Shepherd, G.M., Pologruto, T.A. & Svoboda, K. Circuit analysis of experience-dependent plasticity in the developing rat barrel cortex. *Neuron* **38**, 277–289 (2003).
48. Harris, K.D., Henze, D.A., Csicsvari, J., Hirase, H. & Buzsaki, G. Accuracy of tetrode spike separation as determined by simultaneous intracellular and extracellular measurements. *J. Neurophysiol.* **84**, 401–414 (2000).

doi:1.1038/nn.3078

A toolbox of Cre-dependent optogenetic transgenic mice for light-induced activation and silencing

Linda Madisen[1], Tianyi Mao[2,7], Henner Koch[3], Jia-min Zhuo[4], Antal Berenyi[5], Shigeyoshi Fujisawa[5], Yun-Wei A. Hsu[3], Alfredo J. Garcia III[3], Xuan Gu[4], Sebastien Zanella[3], Jolene Kidney[1], Hong Gu[1], Yimei Mao[4], Bryan M. Hooks[2], Edward S. Boyden[6], György Buzsáki[5], Jan Marino Ramirez[3], Allan R. Jones[1], Karel Svoboda[2], Xue Han[4], Eric E. Turner[3], Hongkui Zeng[1]*

Supplementary Information

Supplementary Figure 1. Baseline fluorescence level in the reporter lines in the absence of Cre, as well as Cre-induced transgene expression in *Pvalb*-IRES-Cre. (**a**) No baseline fluorescence above background in Ai27, Ai32, Ai35 and Ai39 reporter mice alone (without Cre induction). Areas shown: first row, cortex; second row, hippocampus; third row, striatum and thalamus. Scale bar, 200 μm. Bottom row shows confocal images of the CA1 pyramidal neurons. Scale bar, 20 μm. (**b**) Confocal images in the cortex showing Cre-induced transgene expression at native fluorescence level in *Pvalb*+ neurons in *Pvalb*-IRES-Cre;Ai27, *Pvalb*-IRES-Cre;Ai32, *Pvalb*-IRES-Cre;Ai35, *Pvalb*-IRES-Cre;Ai39 mice. White arrowheads point to ring-shaped cell bodies with no intracellular aggregates, indicating protein localization to the cell membrane and processes. Scale bar, 20 μm. Both ChR2-EYFP in Ai32 and Arch-EGFP-ER2 in Ai35 exhibit strong fluorescence, indicating they have high-level protein expression. Strong fluorescence for ChR2-tdTomato in Ai27 was also observed, however, because of the fast bleaching of tdTomato under confocal microscope, the ChR2-tdTomato fluorescence does not appear to be prominent in the image shown. On the other hand, eNpHR3.0-EYFP in Ai39 exhibits significantly weaker fluorescence, indicating lower-level protein expression.

Nature Neuroscience: doi:10.1038/nn.3078

Supplementary Figure 1

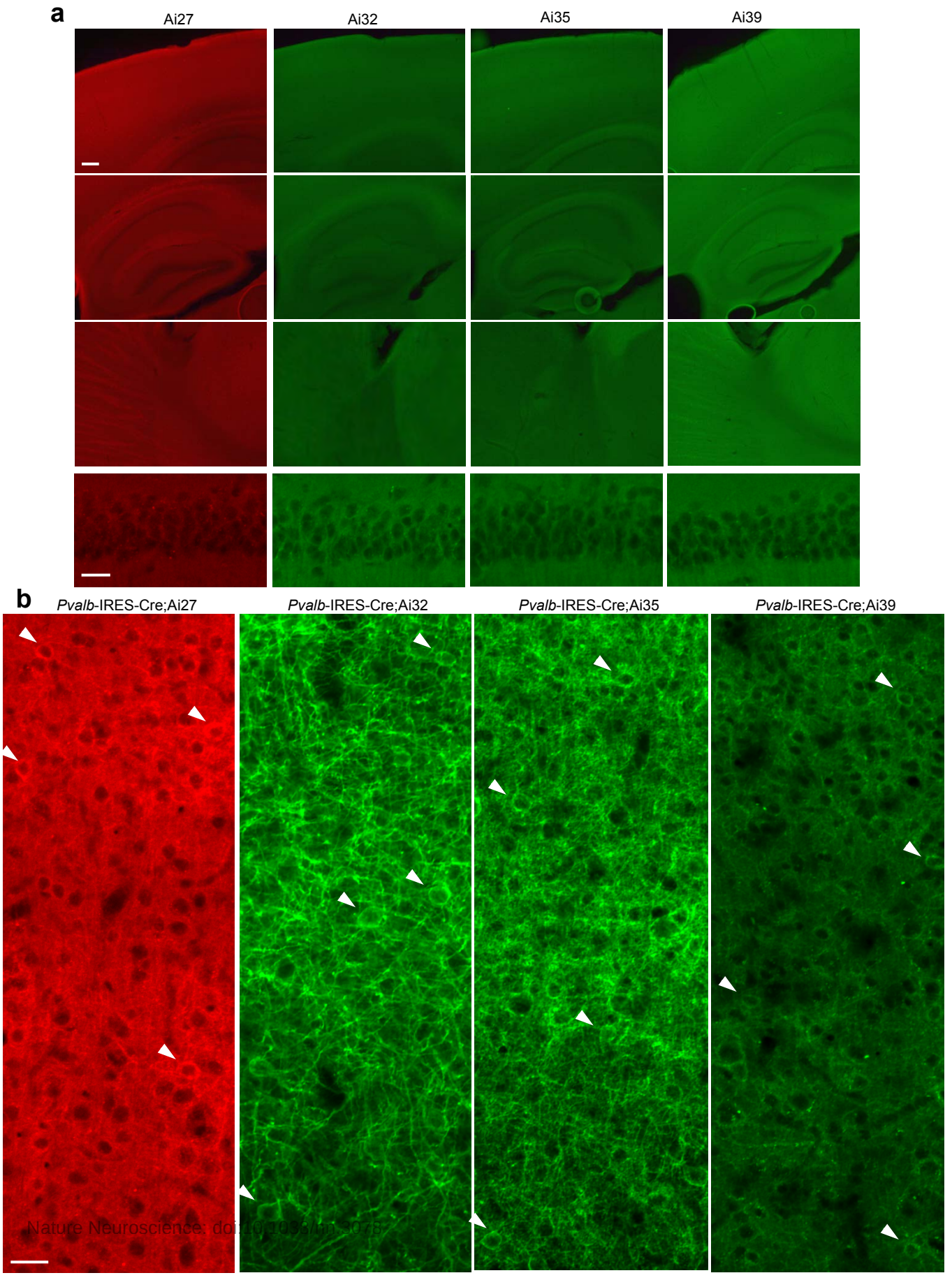

Supplementary Figure 2

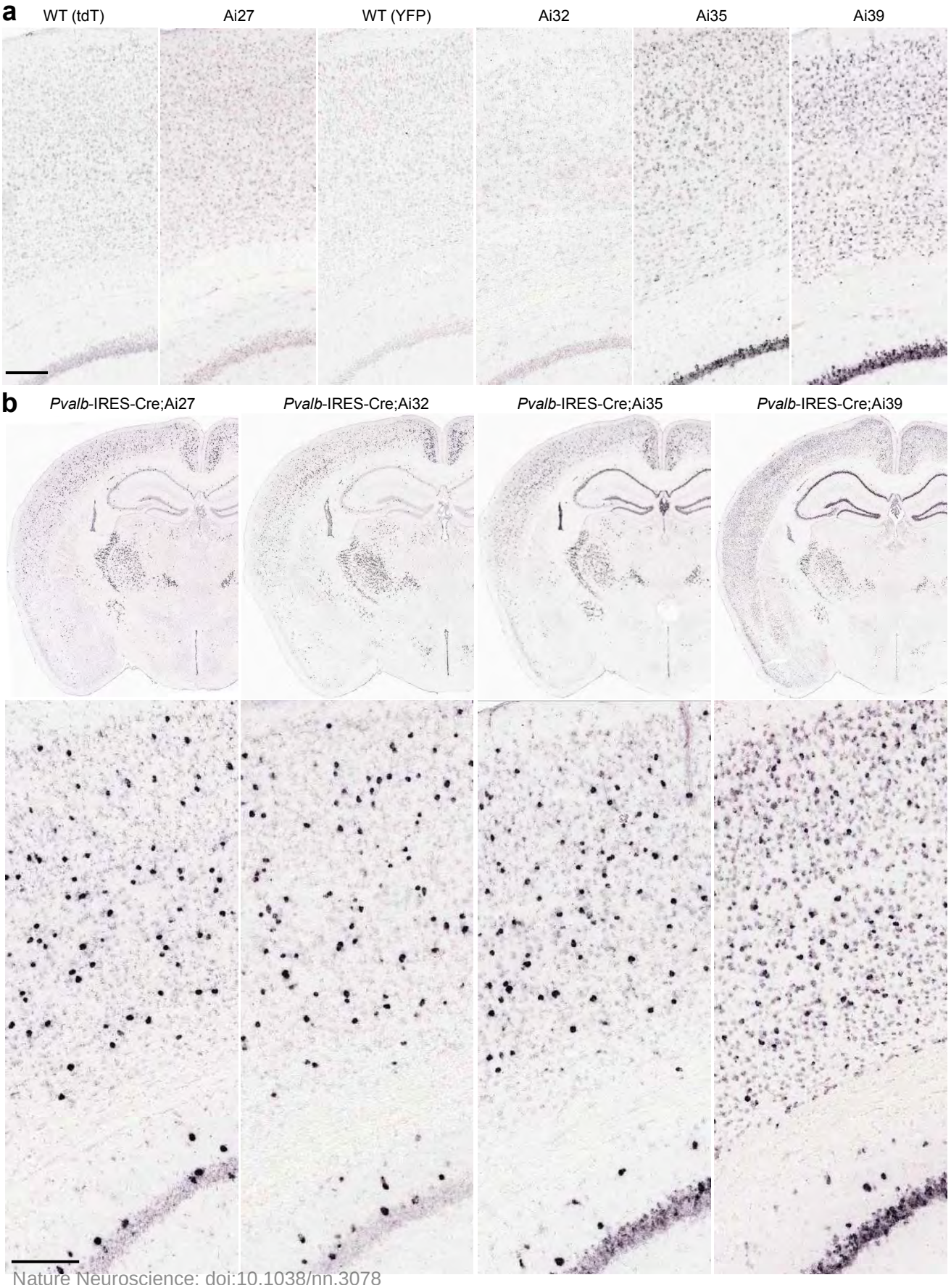

Nature Neuroscience: doi:10.1038/nn.3078

Supplementary Figure 2. Additional ISH expression data showing baseline mRNA levels in the reporter lines in the absence of Cre, as well as Cre-induced mRNA levels in reporters crossed to *Pvalb*-IRES-Cre. (**a**) Baseline mRNA levels in cortex and hippocampus in Ai27, Ai32, Ai35 and Ai39 reporter mice alone (without Cre induction). Wildtype (WT) mouse sections were used as negative controls for the tdTomato (tdT) probe used in Ai27 and the EYFP probe used in Ai32, Ai35 and Ai39. Leaky expression in these areas at the mRNA level was observed in Ai35 mice at low level (mainly in hippocampus), and in Ai39 mice at significant level (mainly in cortex and hippocampus) (also observable in **b**). Although the cause of this unexpected leakage in only certain lines is unknown, as the sequences of the targeting vectors were identical except for the transgenes themselves and their neighboring restriction sites for cloning, one possibility might be that there is cryptic transcriptional start or splicing acceptor site(s) in the transgene sequence that could lead to low-level skipping of the stop cassette in front of the transgene. (**b**) Strong Cre-induced transgene expression at mRNA levels in *Pvalb*+ neurons in *Pvalb*-IRES-Cre;Ai27, *Pvalb*-IRES-Cre;Ai32, *Pvalb*-IRES-Cre;Ai35, *Pvalb*-IRES-Cre;Ai39 mice (ages P148-151). Note the substantially higher signals in targeted cells above the baseline background in each mouse line. Scale bars, 200 μm.

Supplementary Figure 3. Additional ISH expression data showing strong Cre-induced transgene expression throughout the brain. The ages of all mice used were ~P56. (**a**) ChR2-tdTomato mRNA expression in cholinergic neurons in the basal forebrain (middle panel) and brainstem (bottom panel) in *Chat*-IRES-Cre;Ai27 mice. (**b**) ChR2-EYFP mRNA expression in cholinergic neurons in the basal forebrain (middle panel) and brainstem (bottom panel) in *Chat*-IRES-Cre;Ai32 mice. (**c**) Arch-EGFP-ER2 mRNA expression in widespread brain regions, including cortex (middle panel), striatum and thalamus (both shown in bottom panel) in *Camk2a*-CreERT2;Ai35 mice after tamoxifen induction. (**d**) eNpHR3.0-EYFP mRNA expression in widespread brain regions, including cortex (middle panel), striatum and thalamus (both shown in bottom panel) in *Camk2a*-CreERT2;Ai39 mice after tamoxifen induction. Scale bar, 200 μm.

Nature Neuroscience: doi:10.1038/nn.3078

Supplementary Figure 3

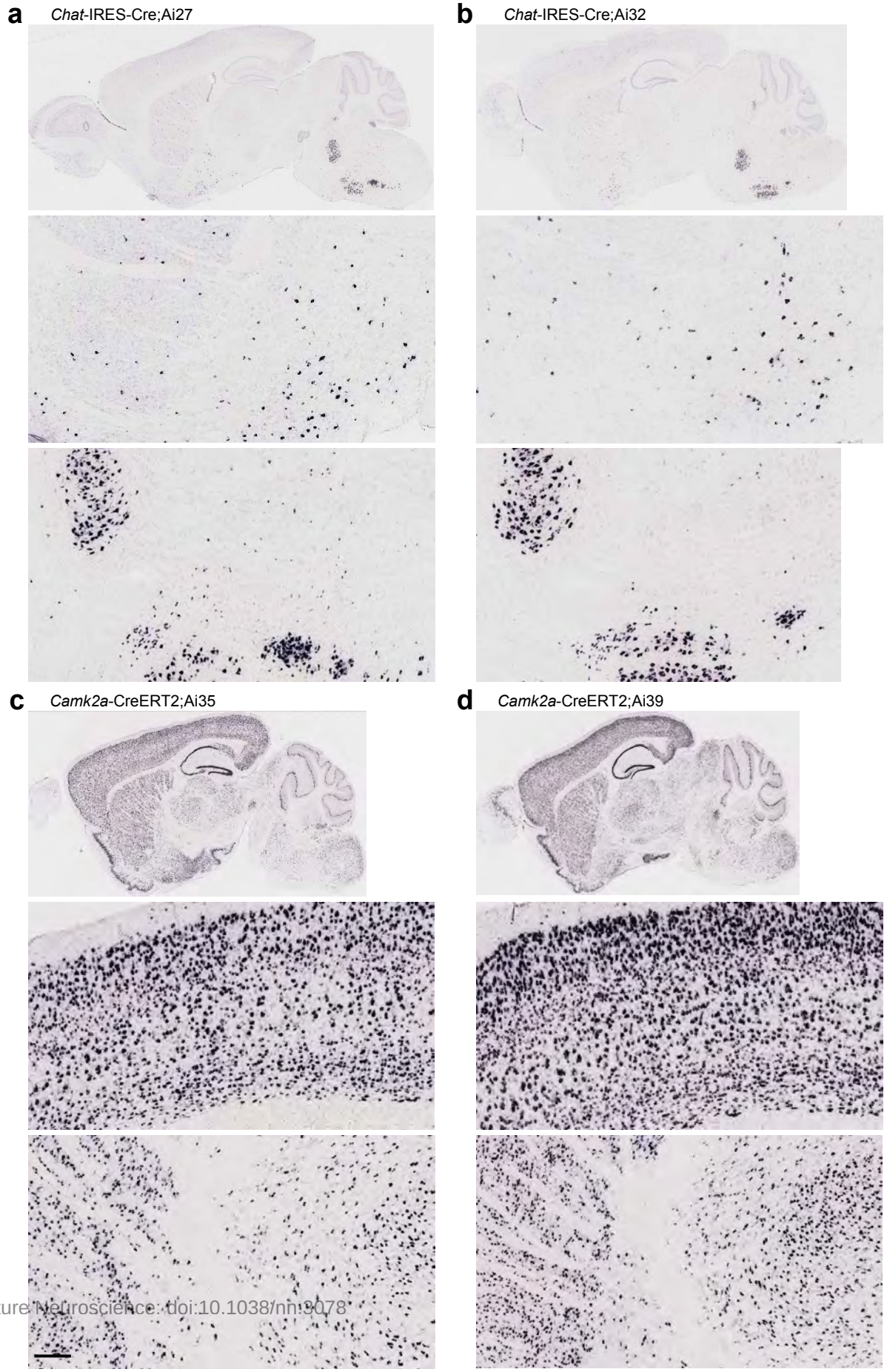

Supplementary Figure 4

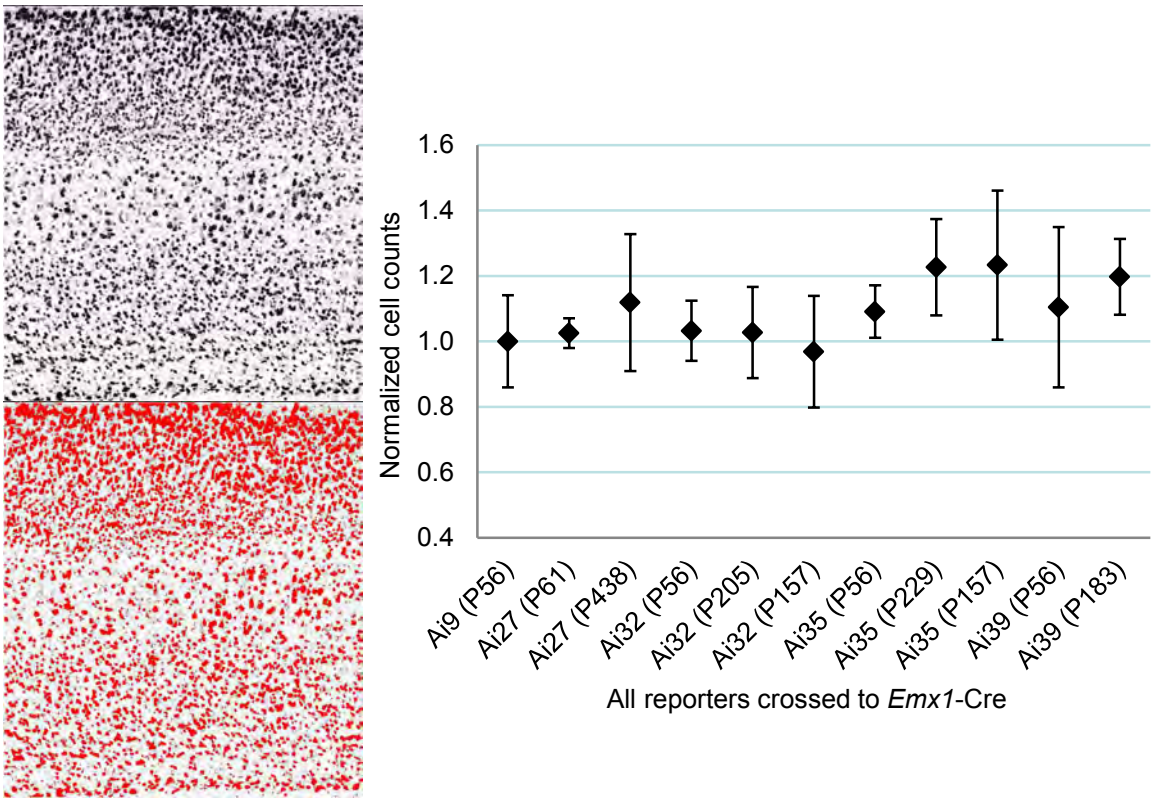

Supplementary Figure 4. Quantification of the number of Cre-induced reporter-expressing cells from reporter ISH images in the cortex of *Emx1*-Cre;Ai27, *Emx1*-Cre;Ai32, *Emx1*-Cre;Ai35 and *Emx1*-Cre;Ai39 mice of various ages. Each data point represents the average cell count from one mouse. For each line, one younger mouse (P56 or P61) and 1-2 older mice (P157-P438, oldest available ones in our mouse colony at the time of experiment) were used for the cell counting. A P56 *Emx1*-Cre;Ai9 mouse was used as control (Ai9: the tdTomato-expressing Cre reporter [9]). Although not fully shown here, the reporter ISH pattern of every mouse used appeared identical to that shown in **Figure 1d**. For counting of transgene-expressing cells, 3 ROIs (regions of interest) spanning the entire cortical depth were chosen, one each from motor, somatosensory or visual cortical area. The number of expressing cells in each ROI was estimated using the Analyze Particles application in the Fiji image analysis software. One example ROI (from the oldest mouse, P438 *Emx1*-Cre;Ai27) is shown here. Upper panel is the raw ISH image, and lower panel is the image after thresholding with particles to be counted highlighted in red. Normalized cell counts (Y-axis) refer to the average cell count per unit area for each mouse normalized to that of the *Emx1*-Cre;Ai9 control mouse which was set to 1. Each data point is mean ± s.d. There is no significant difference between *Emx1*-Cre;Ai9 and any of the other mouse ($p > 0.1$, unpaired student's t-test). The normal ISH expression pattern and normal cell counts for all these mice indicate that long-term expression of all the optogenetic molecules at levels attained in these transgenic lines did not have toxicity.

Nature Neuroscience: doi:10.1038/nn.3078

Supplementary Figure 5

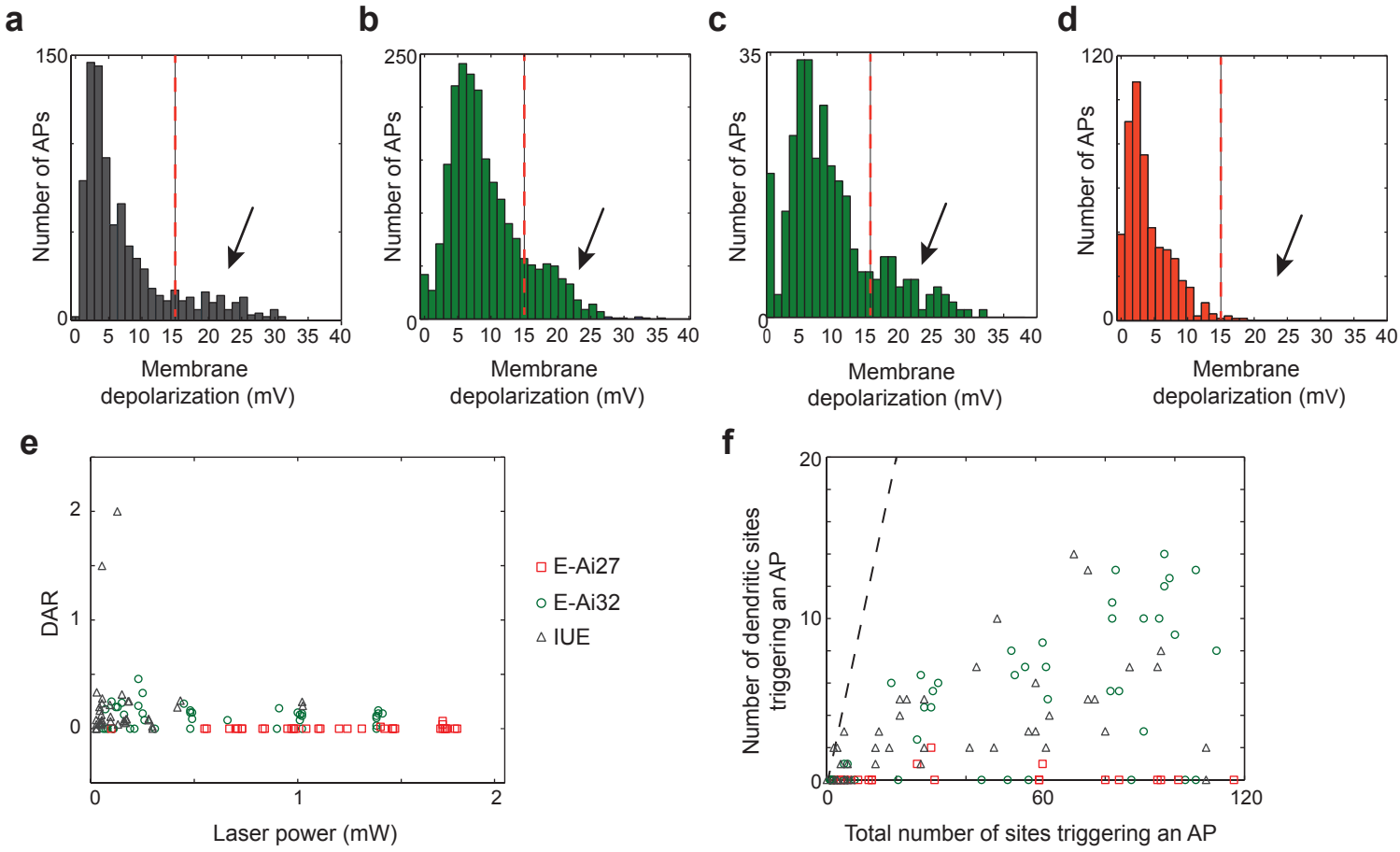

Supplementary Figure 5. Preferential photoexcitability in dendrites or axons of *Emx1*-Cre;Ai27 (abbreviated as E-Ai27) and *Emx1*-Cre;Ai32 (abbreviated as E-Ai32) mice. (**a-d**) Histograms of membrane potentials at the inflection points (also see Methods) for (**a**) *in utero* electroporated (IUE) cells (n = 6), (**b**) E-Ai32 cells (n = 9), (**c**) E-Ai32 cells around threshold laser power (n = 9, laser power 30-200 μW), and (**d**) E-Ai27 cells (n = 12). For each cell, responses from all laser power stimulations are included. Red dashed lines indicate the threshold (15 mV) for determining axonal versus somatic/dendritic responses. Somatic/dendritic components are indicated by arrows. In both ChR2-Venus IUE cells (**a**) and E-Ai32 cells (**b, c**), more AP events had pre-spiking membrane potentials greater than the 15-mV threshold, indicating a somatic/dendritic component that was nearly absent in E-Ai27 cells (**d**). (**e**) The ratio of the number of the photostimulation sites triggering action potentials in somata and dendrites to the number of sites triggering action potentials in axons (DAR) plotted against the laser power used for photostimulation. Green circles: E-Ai32 cells; red squares: E-Ai27 cells; gray triangles: ChR2-Venus IUE cells. Each point represents DAR calculated from one trial in the corresponding animal group. (**f**) The number of the photostimulation sites triggering action potentials in somata and dendrites plotted against the total number of photostimulation sites triggering action potentials. The black dotted line (slope of 1) indicates the positions when all stimulation sites are somatic/dendritic.

Supplementary Figure 6

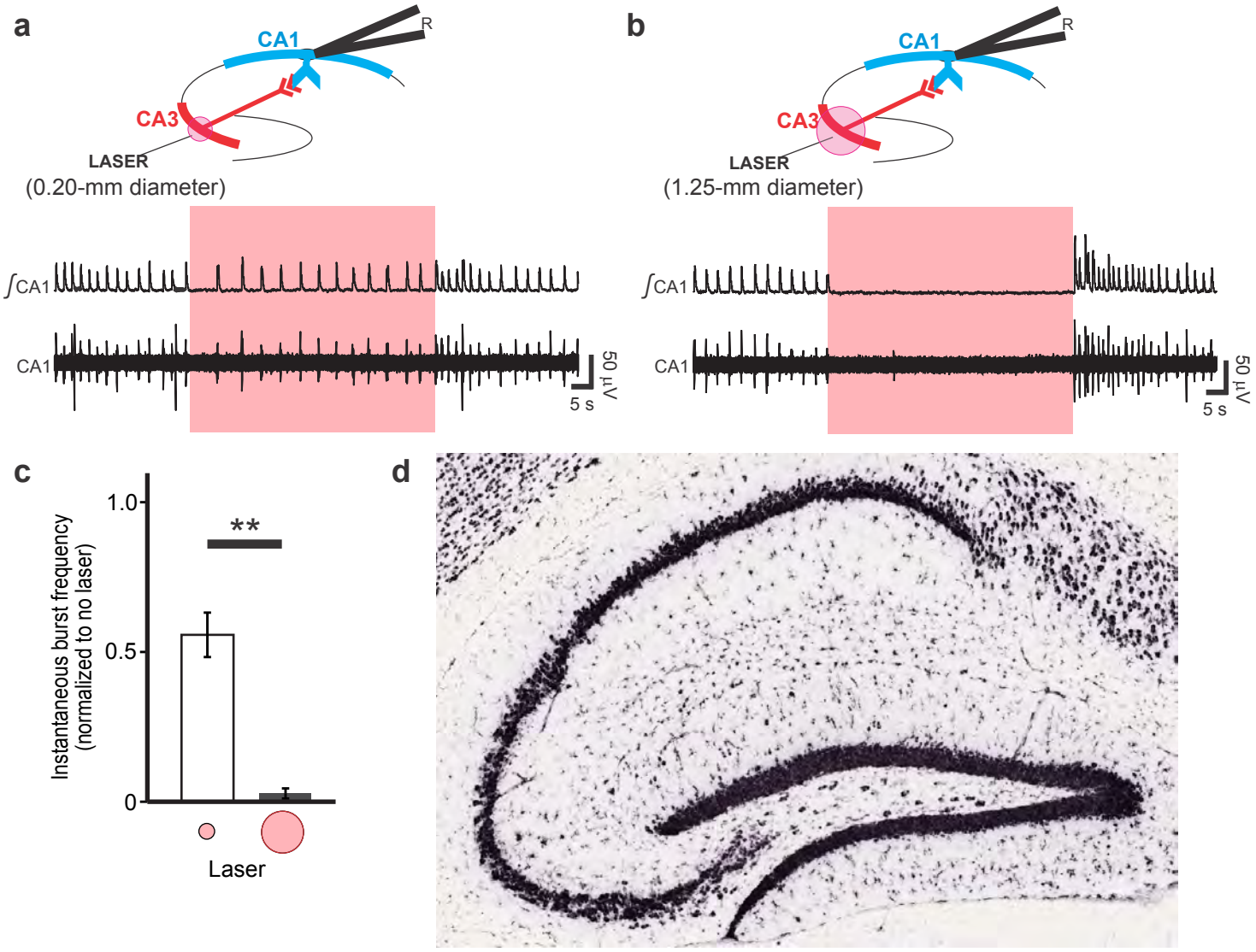

Supplementary Figure 6. Inhibition of the hippocampal network in *Emx1*-Cre;Ai35 mice is dependent on the area of illumination of CA3. The experimental design was similar to that in **Figure 5**, in which activity in CA1 was inhibited by optogenetic silencing of CA3. However, in this experiment, a laser (640 nm) was used instead of an LED to give more precise control over the area of illumination, and the total light power was varied to maintain constant illumination per unit area (35 mW mm^{-2}) while the area was varied by changing the distance from the end of the optical fiber to the surface of the slice. Adult mice approximately 6 months of age were used. (**a**) Illumination of a 0.20-mm diameter area of CA3 reversibly attenuated, but did not completely inhibit, postsynaptic bursting of area CA1 neurons. (**b**) Increasing the diameter of the area of illumination to 1.25 mm of CA3 resulted in nearly complete inhibition of the postsynaptic bursting of area CA1 neurons, but still allowed reversal, with some rebound increase in activity noted. (**c**) Summary of the degree of laser-mediated inhibition of postsynaptic CA1 neuronal bursting based on the instantaneous frequency of population bursting normalized to the period prior to laser exposure, for three separate trials. Smaller circle (left) represents a light zone with a 0.20-mm diameter (n = 3). Larger circle (right) represents a light zone with a 1.25-mm diameter (n = 3). Increasing the diameter of the light zone significantly increases the degree of inhibition in area CA1 (** $p < 0.01$, paired student's t-test). Data expressed as mean ± s.d. (**d**) Reporter transgene expression by ISH in the hippocampus of *Emx1*-Cre;Ai35 mouse, showing near 100% expression in the excitatory neurons in the CA1, CA3 and dentate gyrus subfields.

Nature Neuroscience: doi:10.1038/nn.3078

Supplementary Figure 7

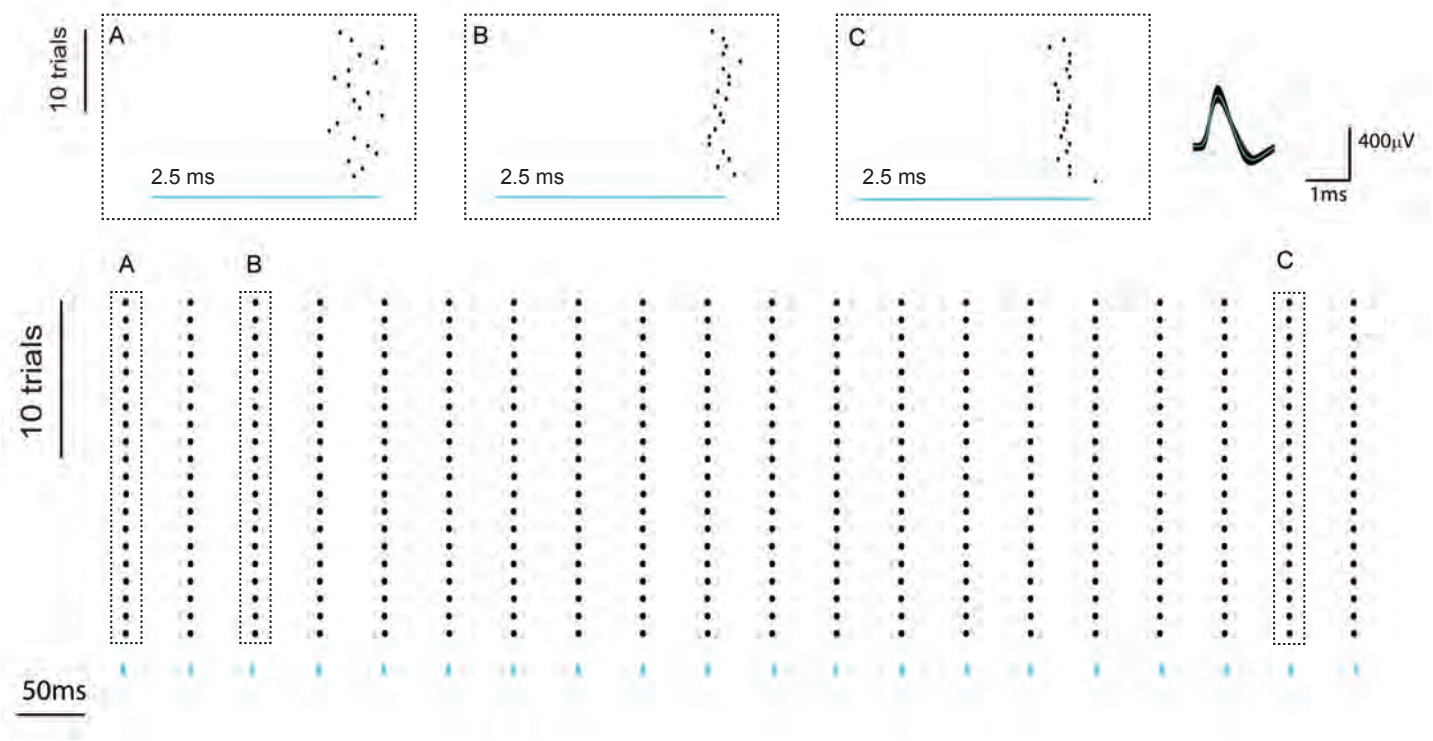

Supplementary Figure 7. Light evoked spiking in *Emx1*-Cre;Ai32 mouse with the sub-millisecond temporal precision. Spike raster plot and waveforms in a representative neuron upon blue light illumination (20-Hz pulse trains with 2.5-ms pulses, ~3 mW mm^{-2} at the optical fiber tip which is ~500 μm above recording electrode). The upper inserts A, B and C demonstrate the timing of each spike upon illumination by the 1st, 3rd, and 19th pulse of the light pulse train, across 20 repetitions.

Supplementary Figure 8

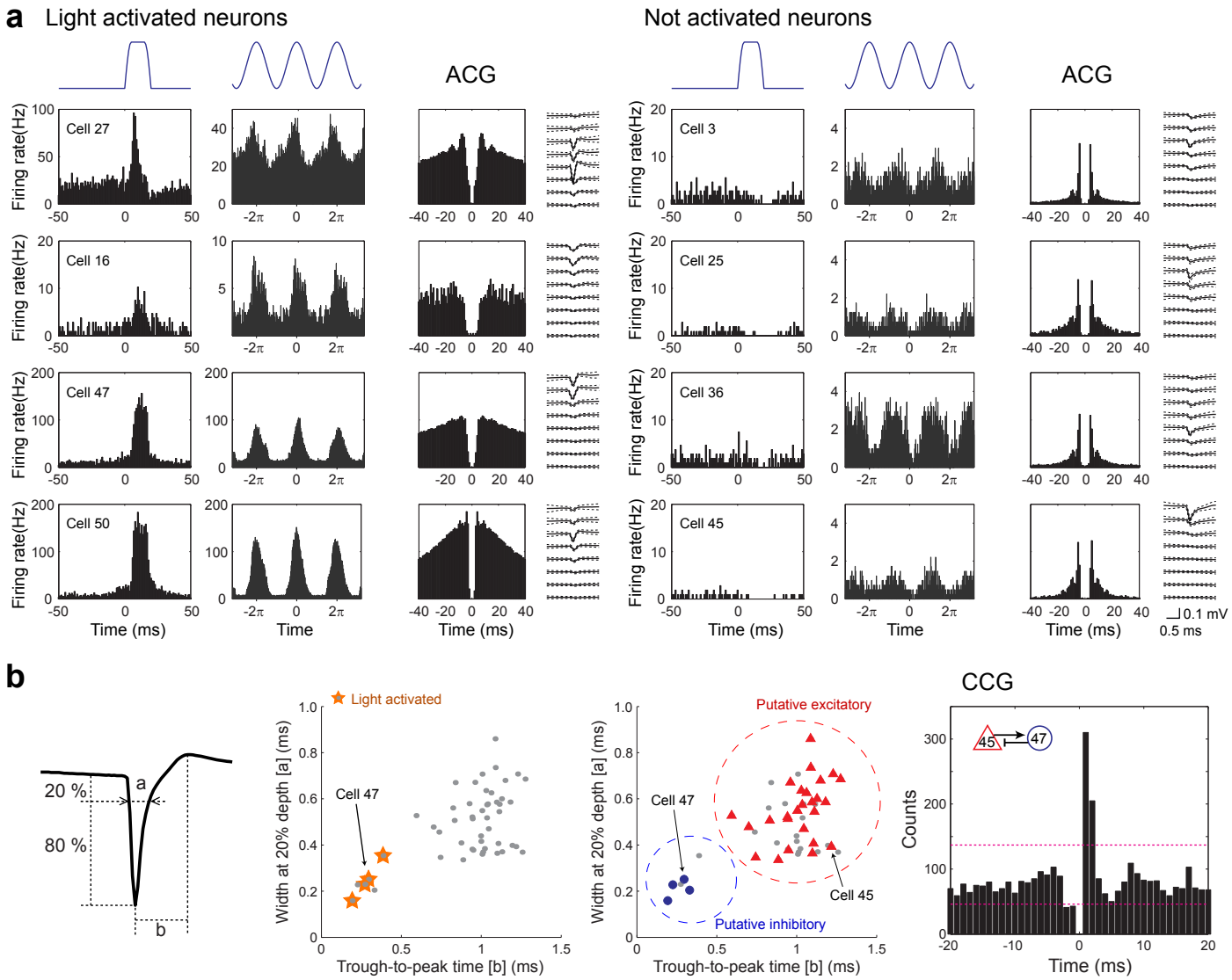

Supplementary Figure 8. Excitation of ChR2-expressing neurons in the hippocampal CA1 of *Pvalb*-IRES-Cre;Ai32 mice during waking state. (**a**) PSTHs of example neurons (additional to **Fig. 7a**), which were transiently activated (left 4 neurons) and transiently suppressed (right 4 neurons) by a single light pulse and sinus (8 Hz) stimulation. Autocorrelogram (ACG) and waveform of each neuron are also shown. Light intensity was 1 mW. (**b**) Physiological and optogenetic classification of neuron types in the hippocampus. Left panel, spike width and trough-to-peak time of the wide-band (1 Hz - 5 kHz) waveform of pyramidal neuron spikes. Middle panels, segregation of simultaneously recorded neurons by these two parameters. Middle left, light-activated neurons are marked with orange stars. Middle right, putative pyramidal cells and interneurons are indicated in the same plot as middle left. Red triangles and blue circles (Middle panels) indicate excitatory and inhibitory neurons identified by monosynaptic interactions, calculated from their cross-correlogram (Right panel). Note strong overlap between the physiologically characterized groups and the optogenetically characterized groups.

Nature Neuroscience: doi:10.1038/nn.3078

Supplementary Figure 9

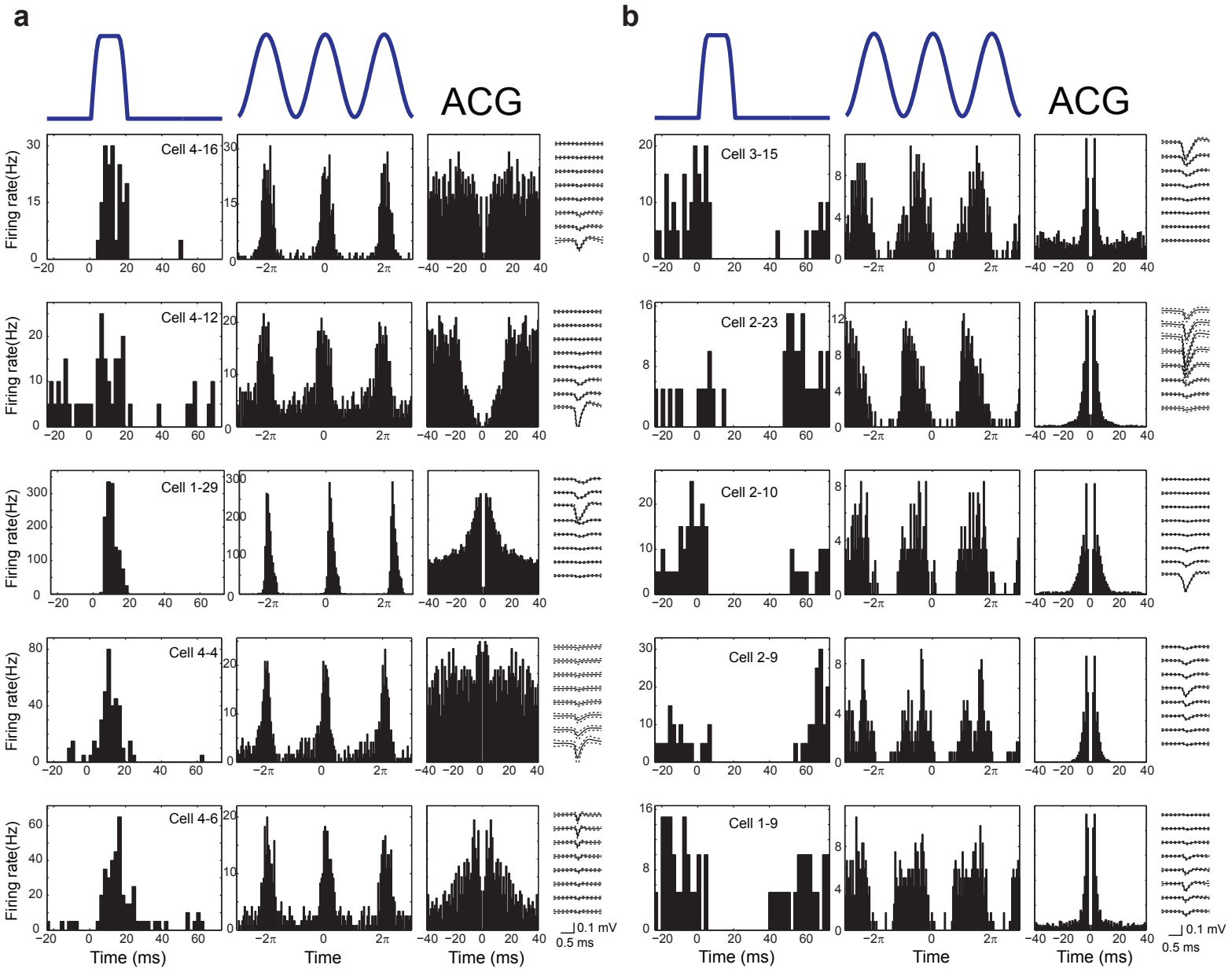

Supplementary Figure 9. Light activation of *Pvalb*+ neurons in the reticular nucleus of the thalamus in the *Pvalb*-IRES-Cre;Ai32 mice (providing additional examples to **Fig. 7c**). (**a**) Each row is an activated reticular neuron. Evoked responses by single pulse (20 ms) or sinus (10 Hz) stimulation, ACG, and mean waveform of the neurons recorded at each of the 8 sites of the silicon probe shank (4-shank probes were used to record simultaneously from both reticular nucleus and neighboring ventrolateral nucleus of thalamus). (**b**) Same arrangement, showing 5 example thalamocortical neurons. Note ACG typical of bursting thalamocortical cells and their difference from the light-activated reticular neurons.

Nature Neuroscience: doi:10.1038/nn.3078